MBoC | ARTICLE

The RNA-binding protein Nab2 regulates levels of the RhoGEF Trio to govern axon and dendrite morphology

Carly L. Lancaster[a,b,c], Pranav S. Yalamanchili[a,b], Jordan N. Goldy[a,b,c], Sara W. Leung[a], Anita H. Corbett[a,*], and Kenneth H. Moberg[b,*]

[a]Department of Biology, Emory College of Arts and Sciences, Atlanta, GA 30322; [b]Department of Cell Biology, Emory University School of Medicine, Atlanta, GA 30322; [c]Graduate Program in Biochemistry, Cell and Developmental Biology, Emory University, Atlanta, GA 30322

ABSTRACT **The *Drosophila* RNA-binding protein (RBP) Nab2 acts in neurons to regulate neurodevelopment and is orthologous to the human intellectual disability-linked RBP, ZC3H14. Nab2 governs axon projection in mushroom body neurons and limits dendritic arborization of class IV sensory neurons in part by regulating splicing events in ~150 mRNAs. Analysis of the *Sex-lethal* (*Sxl*) mRNA revealed that Nab2 promotes an exon-skipping event and regulates m^{6}A methylation on *Sxl* pre-mRNA by the Mettl3 methyltransferase. Mettl3 heterozygosity broadly rescues *Nab2^{null}* phenotypes implying that Nab2 acts through similar mechanisms on other RNAs, including unidentified targets involved in neurodevelopment. Here, we show that Nab2 and Mettl3 regulate the removal of a 5′UTR (untranslated region) intron in the *trio* pre-mRNA. Trio utilizes two GEF domains to balance Rac and RhoGTPase activity. Intriguingly, an isoform of Trio containing only the RhoGEF domain, GEF2, is depleted in *Nab2^{null}* nervous tissue. Expression of Trio-GEF2 rescues projection defects in *Nab2^{null}* axons and dendrites, while the GEF1 Rac1-regulatory domain exacerbates these defects, suggesting Nab2-mediated regulation Trio-GEF activities. Collectively, these data indicate that Nab2-regulated processing of *trio* is critical for balancing Trio-GEF1 and -GEF2 activity and show that Nab2, Mettl3, and Trio function in a common pathway that shapes axon and dendrite morphology.**

SIGNIFICANCE STATEMENT

- *Drosophila* Nab2, orthologue of the human RBP ZC3H14 lost in inherited intellectual disability, acts through unknown RNA targets to control axon and dendrite morphology.
- This study shows that Nab2 and the Mettl3 methyltransferase guide splicing of trio mRNA, which encodes a conserved GEF-domain protein. Loss of Nab2 is associated with an imbalance in levels of Trio GEF domains in Nab2-deficient neurons. Restoring this balance partially rescues neuronal defects.
- These findings suggest that Nab2 control of Trio levels is required to pattern axon and dendrite growth and suggests that ZC3H14 may play a similar role in the vertebrate brain.

Monitoring Editor
Avital Rodal
Brandeis University

Received: Apr 5, 2024
Revised: Jun 17, 2024
Accepted: Jul 2, 2024

Cross-Validation

New Hypothesis

This article was published online ahead of print in MBoC in Press (http://www.molbiolcell.org/cgi/doi/10.1091/mbc.E24-04-0150) on July 10, 2024.

Conflict of interest: The authors declare no financial conflict of interest.

Author contributions: C.L., S.L., A.C., and K.M. conceived and designed the experiments; C.L. and P.Y. performed the experiments; C.L., P.Y., and J.G. analyzed the data; C.L., A.C., and K.M. drafted the article; C.L. prepared the digital images; C.L., A.C., and K.M. other.

*Address correspondence to: Anita H. Corbett (acorbe2@emory.edu); Kenneth H. Moberg (kmoberg@emory.edu).

Abbreviations used: GEF, guanine nucleotide exchange factor.; Nab2, nuclear polyadenosine RNA-binding protein 2; Pab, polyadenosine binding protein; RBP, RNA-binding protein; ZC3H14, zinc finger Cys-Cys-Cys His type containing 14.

INTRODUCTION

RNA-binding proteins (RBPs) associate with nascent RNA transcripts and govern expression via a multitude of mechanisms, including regulation of splicing, polyadenylation, nuclear export, translation, and stability (Maniatis and Reed, 2002; McKee and Silver, 2007; Corbett, 2018; Corley *et al*., 2020). These RNA–RBP interactions are particularly important in highly specialized cells such as neurons which require fine-tuned spatiotemporal control of gene expression to ensure proper development and function of the nervous system (Bardoni *et al.*, 2012; Santoro *et al.*, 2012; Conlon and Manley, 2017; Thelen and Kye, 2019; Gebauer *et al.*, 2021). The importance of RBP function in neurons is highlighted by the prevalence of neurodevelopmental diseases that have been linked to defects in RBPs, leading to aberrant processing of RNAs encoding neurodevelopment factors (Cooper *et al*., 2009; Pak *et al.*, 2011; Bardoni *et al.*, 2012; Darnell and Richter, 2012; Gross *et al*., 2012; Santoro *et al.*, 2012; Edens *et al.*, 2015; Agrawal *et al.*, 2019). Intriguingly, many of these RBPs are ubiquitously expressed and have roles in relatively common RNA processing mechanisms (Barbe *et al*., 1996; Franke *et al*., 1996; Brais, 2003; Lage *et al.*, 2008; Kolb and Kissel, 2011; Pirozzi *et al*., 2011). Therefore, defining roles for these RBPs in neurons has become key to understanding why they are linked to neurological disease.

One important family of posttranscriptional regulatory proteins consists of polyadenosine binding proteins (Pabs) (Kelly *et al*., 2010). Conventional Pab family members bind polyadenosine RNA via RNA recognition motifs and modulate a multitude of RNA processing events such as splicing, export, polyadenylation, translation, and stability (Banerjee *et al*., 2013; Goss and Kleiman, 2013; Wigington *et al.*, 2014). Another less well-studied group of Pabs utilize zinc finger (ZnF) domains to bind specific RNA motifs and modulate downstream processing events (Kelly *et al*., 2007; Kelly *et al.*, 2010; Kelly *et al*., 2014). One such ZnF Pab termed zinc finger Cys-Cys-Cys-His-type containing 14 (ZC3H14; also termed MSUT2) is expressed ubiquitously and binds tracts of polyadenosine RNA with high affinity via tandem ZnF domains (Kelly *et al.*, 2007; Leung *et al*., 2009; Kelly *et al.*, 2010; Kelly *et al*., 2014; Wheeler *et al*., 2019). Despite ubiquitous expression, mutations in human *ZC3H14* cause a form of inherited nonsyndromic autosomal recessive intellectual disability, which implies a specific requirement for ZC3H14 in the developing brain (Pak *et al*., 2011; Kelly *et al*., 2012).

The ZC3H14 protein is evolutionarily conserved among eukaryotes and has been studied in *Mus musculus* (*Zc3h14*) (Guthrie *et al*., 2011; Pak *et al*., 2011; Soucek *et al*., 2016), *Caenorhabditis elegans* (*sut-2*) (Guthrie *et al*., 2009), *Sacchromyces cerevisiae* (Nab2) (Anderson *et al*., 1993; Green *et al*., 2002; Hector *et al*., 2002; Marfatia *et al*., 2003; Kelly *et al*., 2007; Kelly *et al*., 2010; Schmid *et al*., 2015; Soucek *et al*., 2016), *Sacchromyces pombe* (Nab2) (Grenier St-Sauveur *et al*., 2013), and *Drosophila melanogaster* (Nab2) (Pak *et al*., 2011; Kelly *et al*., 2016; Fasken *et al*., 2019; Lee *et al*., 2020; Corgiat *et al*., 2021; Corgiat *et al*., 2022; Rounds *et al*., 2022; Jalloh *et al*., 2023). These studies have collectively uncovered molecular and neuronal functions for this conserved ZnF Pab. For example, *Zc3h14* loss impairs working memory in mice where ZC3H14 protein localizes to synaptosomes in hippocampal neurons and regulates the abundance of synaptic proteins, including CaMK2α (Rha *et al*., 2017; Jones *et al*., 2020). Moreover, studies in *C. elegans* identified SUT-2 as a modulator of Tau-induced toxicity, as loss of *sut-2* robustly rescues the toxic consequences of Tau overexpression in worms (Guthrie *et al*., 2009; Currey *et al*., 2023), a function of ZC3H14/MSUT2 that extends to mice (McMillan *et al*., 2021). On the other hand, yeast *NAB2* is essential for viability (Anderson *et al*., 1993) and has critical functions in regulating transcription termination (Alpert *et al*., 2020), nuclear export (Hector *et al*., 2002), and transcript stability (Batisse *et al*., 2009; Schmid *et al*., 2015; Fasken *et al*., 2019; Alpert *et al*., 2020). Moreover, *NAB2/Nab2* loss leads to increases in bulk poly(A) tail length in yeast, mice, and flies supporting a conserved function for Nab2 in restricting poly(A) tail length (Green *et al*., 2002; Hector *et al*., 2002; Kelly *et al*., 2010; Kelly *et al*., 2014). Taken together, these findings suggest that ZC3H14/Nab2 is involved in multiple aspects of posttranscriptional RNA metabolism and that these roles may be particularly significant in neurons.

D. melanogaster is a genetically tractable system in which to define molecular and developmental roles of the ZC3H14 invertebrate homologue, Nab2 (Pak *et al*., 2011). Our prior studies have determined that Nab2 function is necessary in neurons, as pan-neuronal expression of *Drosophila* Nab2 or human ZC3H14 is sufficient to rescue viability and locomotor defects associated with zygotic loss of Nab2 (Pak *et al*., 2011; Kelly *et al*., 2014). Moreover, Nab2 has a cell-autonomous role in Kenyon cells to pattern axonal projections from these cells into the mushroom bodies (Kelly *et al*., 2016), a twin neuropil structure that regulates *Drosophila* associative olfactory learning and memory (Heisenberg, 2003; Kahsai and Zars, 2011; Yagi *et al*., 2016; Takemura *et al*., 2017). Biochemical studies show that Nab2 interacts with Fmr1, the fly homolog of Fragile X Syndrome RBP, FMRP (Wan *et al*., 2000), and that these two RBPs coregulate mushroom body morphology and olfactory memory through a mechanism likely to involve translational repression of shared Nab2-Fmr1 target RNAs (Bienkowski *et al*., 2017). Beyond the brain, Nab2 limits dendritic branching of class IV dorsal dendritic arborization (ddaC) sensory neurons through a mechanism involving the planar cell polarity (PCP) pathway (Corgiat *et al*., 2022), suggesting that Nab2 controls RNA targets encoding regulators of the actin cytoskeleton. Our recent work studying the effect of Nab2 loss on the brain transcriptome revealed that Nab2 is required for proper splicing of ~150 mRNAs (Jalloh and Lancaster *et al*., 2023). Furthermore, Nab2 limits methylation at the N-6 position of adenosine (m^6A) on key mRNAs, including the alternatively spliced *Sex-lethal* (*Sxl*) transcript (Jalloh and Lancaster *et al*., 2023). However, Nab2-regulated transcripts encoding factors that guide axon and dendrite morphology have not been identified.

A recent study uncovered multiple Nab2-regulated candidate transcripts with key functions in neurodevelopment (Jalloh and Lancaster *et al*., 2023). Specifically, this work revealed significant retention of a 5′UTR intron in the *trio* transcript. Trio is a member of the Dbl homology (DH) family of guanine nucleotide exchange factor (GEF) proteins with well-conserved orthologues in *C. elegans* and mammals that control F-actin polymerization through the Rac and Rho small GTPases (Bellanger *et al*., 1998b; Awasaki *et al*., 2000; Bateman *et al*., 2000; Newsome *et al*., 2000; Bateman and Van Vactor, 2001; Briancon-Marjollet *et al*., 2008; Ba *et al*., 2016; Pengelly *et al*., 2016; Katrancha *et al*., 2017; Backer *et al*., 2018; Bircher and Koleske, 2021). As a result of these roles, Trio loss affects axon guidance and dendritic branching as well as synaptic transmission and plasticity (Briancon-Marjollet *et al*., 2008; Iyer *et al*., 2012; DeGeer *et al*., 2015; Ba *et al*., 2016; Katrancha *et al*., 2019). Notably, *Drosophila* Trio is enriched in the brain mushroom bodies where it controls axon projection and Trio also regulates arborization of sensory ddaC neurons in the larval peripheral nervous system (PNS) (Awasaki *et al*., 2000; Iyer *et al*., 2012; Shivalkar and Giniger, 2012). Moreover, several recent studies have identified loss- and gain-of-function mutations in the human *TRIO* gene and its paralogue *KALRN* that lead to genetically dominant forms of intellectual

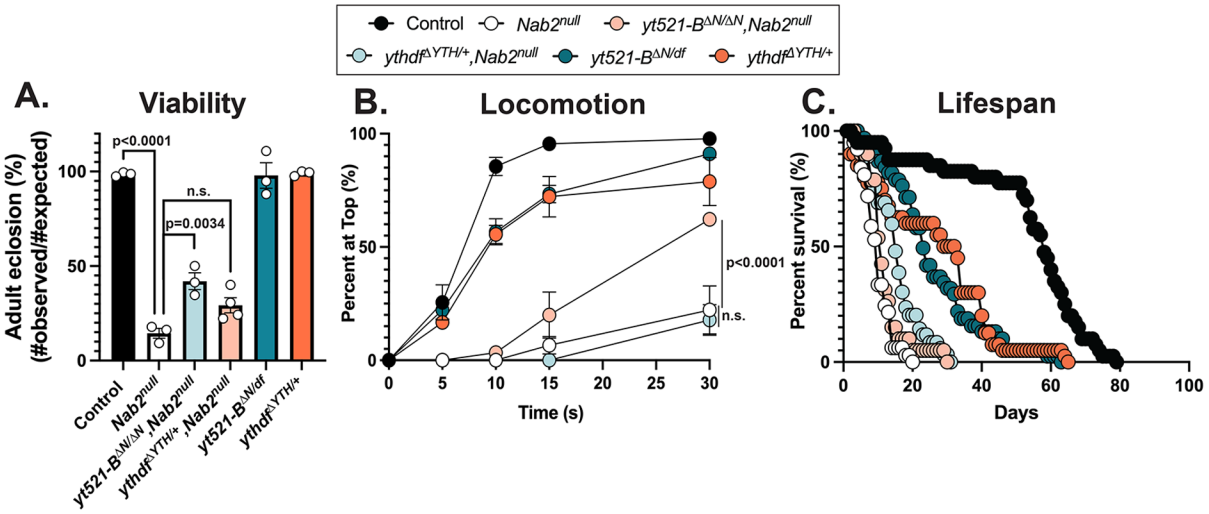

FIGURE 1: Loss of m^{6}A-reader proteins rescues *Nab2*^{null} defects in viability and adult locomotion. (A) Percent of control, *Nab2*^{null}, *yt521-B*$^{\Delta N/\Delta N}$*Nab2*^{null}, *ythdf*$^{\Delta YTH/+}$*Nab2*^{null}, *yt521-B*$^{\Delta N/df}$, and *ythdf*$^{\Delta YTH/+}$ that eclose as viable adults (calculated as #observed/#expected). At least 100 larvae were analyzed for each biological replicate. (B) Negative geotaxis as a measure of locomotion of age-matched adult flies of indicated genotypes over time in seconds (s) taken to reach the top of a vial. The negative geotaxis was observed for at least 10 animals for each biological replicate. (C) Survival of age matched adult flies of the indicated genotypes over time in days. The survival of at least 10 flies was observed for each biological replicate. At least three biological replicates were tested for each genotype and experiment. Significance values are indicated.

disability and neurodevelopmental disease (Ba *et al.*, 2016; Pengelly *et al.*, 2016; Katrancha *et al.*, 2017; Paskus *et al.*, 2020).

Trio contains two GEF domains, GEF1 and GEF2, that differentially activate Rac1 or RhoA/Rho1 GTPases, respectively (Debant *et al.*, 1996; Bellanger *et al.*, 1998a; Bellanger *et al.*, 1998b). Trio-GEF1 activation of Rac1 regulates motor neuron axon guidance, cell migration, and axon outgrowth (Bateman *et al.*, 2000; Newsome *et al.*, 2000; Briancon-Marjollet *et al.*, 2008; Peng *et al.*, 2010; Song and Giniger, 2011). Comparatively, little is known about the function of Trio-GEF2; however, recent work suggests that it promotes growth cone collapse through RhoA/Rho1 (Backer *et al.*, 2018). Supporting this model of opposing roles for Trio GEF1 and GEF2 function, studies in *Drosophila* ddaC neurons suggest that Trio promotes dendritic branching via GEF1 and restricts this process via GEF2 (Iyer *et al.*, 2012). Despite insight into Trio GEF specificity for Rac and RhoA/Rho1, how these two opposing Trio activities are modulated within axons and dendrites remains unclear.

Here, we exploit both genetic and molecular approaches to assess the role of Nab2 and the m^{6}A machinery in regulating expression of the neuronally enriched protein Trio in the adult fly brain. Consistent with our previous findings that Nab2 limits m^{6}A methylation on specific transcripts, reduced levels of either *Drosophila* m^{6}A reader protein—the nuclear reader Yt521-B or the cytoplasmic reader Ythdf—is sufficient to rescue *Nab2*^{null} viability and locomotion defects, indicating that m^{6}A-mediated changes in RNA nuclear processing and cytoplasmic metabolism contribute to defects in Nab2 mutants. Focusing on the *trio* mRNA, we find that Nab2 and the m^{6}A methyltransferase, Mettl3, each promote an intron-excision event within the 5′UTR of a *trio* mRNA species encoding only the GEF2 (RhoGEF) domain. Intriguingly, levels of the corresponding Trio-GEF2 protein drop in heads of *Nab2*^{null} but not *Mettl3*^{null} flies, consistent with a model in which Nab2 modulates both nuclear splicing and cytoplasmic metabolism of the GEF2-only variant of *trio* mRNA. Critically transgenic expression of Trio-GEF2 rescues axon projection defects in *Nab2*^{null} mushroom body neurons and class IV ddaC neurons while Trio-GEF1 has the opposite effect of exacerbating *Nab2*^{null} axon projection defects. Together, these data identify Nab2 and Mettl3 as key regulators of *trio* 5′UTR structure and provide evidence that altered expression of Trio-GEF2 contributes to axon and dendrite defects in *Drosophila* lacking Nab2.

RESULTS

Loss of m^{6}A-reader proteins rescues *Nab2*^{null} defects in viability and adult locomotion

Nab2 loss causes severe defects in *Drosophila* viability, adult locomotion, and lifespan (Pak *et al.*, 2011). Building on the previous finding that Nab2 loss elevates m^{6}A methylation on select mRNAs (Jalloh and Lancaster *et al.*, 2023), we hypothesized that some *Nab2*^{null} organismal phenotypes could result from ectopic recruitment of m^{6}A reader proteins onto affected mRNAs. These m^{6}A reader proteins recognize m^{6}A-modified adenosines via a YTH domain (Xu *et al.*, 2014) and act downstream of the methyltransferase machinery to bind and regulate the fate of methylated RNAs (Luo and Tong, 2014; Theler *et al.*, 2014; Xu *et al.*, 2014; Xu *et al.*, 2015; Patil *et al.*, 2018). Unlike more complex mammalian systems, *Drosophila* have a single nuclear m^{6}A reader protein, YT-521-B (or Ythdc1) and a single cytoplasmic m^{6}A reader protein, Ythdf (Haussmann *et al.*, 2016; Kan *et al.*, 2017).

To assess roles of nuclear Yt521-B and cytoplasmic Ythdf in *Nab2* mutant phenotypes, the *yt521-B*$^{\Delta N}$ and *ythdf*$^{\Delta YTH}$ alleles (Lence *et al.*, 2016; Worpenberg *et al.*, 2021) were individually recombined with a zygotic *Nab2*^{null} allele (also known as *Nab2*^{ex3}; imprecise excision of *EP3716*) (Pak *et al.*, 2011) and assessed for effects on viability, adult locomotion, and lifespan. Homozygous double mutant *yt521-B*$^{\Delta N/\Delta N}$, *Nab2*^{null} flies show increase viability compared with *Nab2*^{null} flies indicating that the nuclear m^{6}A reader is required for the effect of Nab2 loss of viability (Figure 1A). The *ythdf*$^{\Delta YTH}$, *Nab2*^{null} double mutants are inviable; furthermore, heterozygous reduction of cytoplasmic Ythdf (*ythdf*$^{\Delta YTH/+}$, *Nab2*^{null}) does not improve *Nab2*^{null} viability (Figure 1A). In contrast, homozygous loss of nuclear Yt521-B has no effect on *Nab2*^{null} locomotion, whereas heterozygous reduction of cytoplasmic Ythdf rescues *Nab2*^{null} climbing rates by

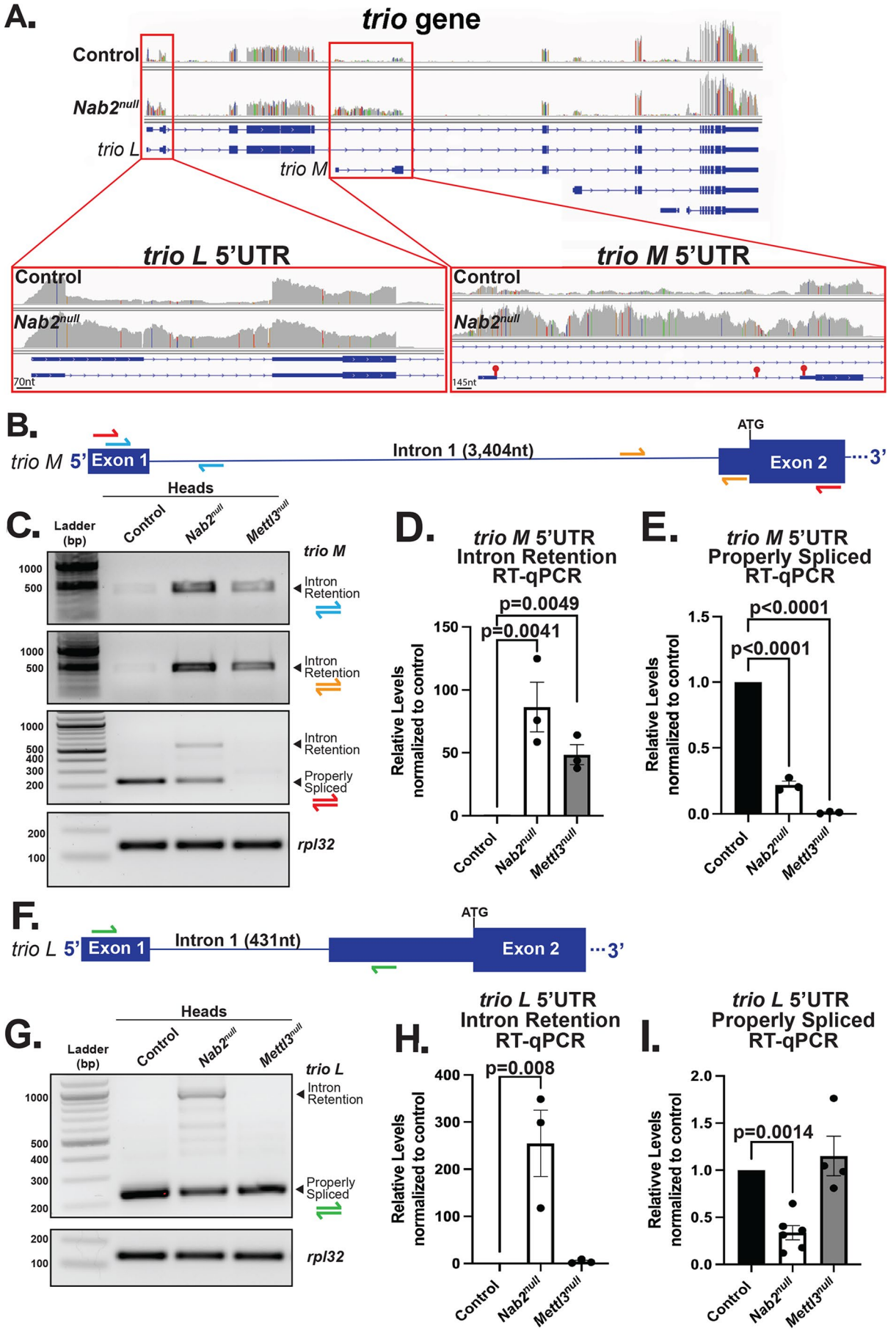
A.
trio gene
Control
Nab2null
trio L
trio M
trio L 5'UTR
trio M 5'UTR
70nt
145nt
B.
trio M 5'
Exon 1
Intron 1 (3,404nt)
ATG
Exon 2
3'
C.
Heads
Ladder (bp)
Control
Nab2null
Mettl3null
trio M
Intron Retention
Properly Spliced
rpl32
D.
trio M 5'UTR Intron Retention RT-qPCR
p=0.0049
p=0.0041
Relative Levels normalized to control
E.
trio M 5'UTR Properly Spliced RT-qPCR
p<0.0001
p<0.0001
F.
trio L 5'
Intron 1 (431nt)
G.
trio L
H.
trio L 5'UTR Intron Retention RT-qPCR
p=0.008
I.
trio L 5'UTR Properly Spliced RT-qPCR
p=0.0014

approximately 6-fold as assessed in a negative geotaxis assay (at the 30 s timepoint; Figure 1B). Despite the ability of reader alleles (e.g., *yt521-B*$^{\Delta N/\Delta N}$ or *ythdf*$^{\Delta YTH/+}$) to rescue viability or adult locomotion, neither mutant alone rescues *Nab2*^{null} lifespan defects (Figure 1C). Together, these genetic rescue data provide evidence that neurological effects of Nab2 loss require nuclear and cytoplasmic m^{6}A readers, and suggest that each of these mechanisms may involve different mRNAs.

Nab2 and Mettl3 regulate splicing of the *trio* 5′UTR in the *Drosophila* head

In light of the effects of Nab2 loss on axon and dendrite development (Kelly *et al.*, 2016; Bienkowski *et al.*, 2017; Rounds *et al.*, 2021; Corgiat *et al.*, 2022), we mined our high-throughput RNA sequencing (RNA-seq) analysis of adult heads from *Nab2*^{null} mutants (zygotic null; imprecise excision of *EP3761*) and isogenic Controls (precise excision of *EP3716*) (Pak *et al.*, 2011; Jalloh and Lancaster *et al.*, 2023) to identify potential Nab2 target transcripts regulated by m^{6}A with functions in neurodevelopment. One transcript identified in this analysis was *trio*, which encodes a Rho guanine nucleotide exchange factor (RhoGEF) that activates specific downstream Rho family GTPases (Bellanger *et al.*, 1998b; Bircher and Koleske, 2021). There are multiple different variants of the *trio* transcript, two of which are readily detected in adult fly heads: hereafter referred to as *trio Medium* (*trio M*) and *trio Long* (*trio L*) (Figure 2A, top panel). Visualization of RNA-seq reads from *Nab2*^{null} and Control heads using Integrative Genomics Viewer (IGV) (Robinson *et al.*, 2017) reveals an increase in reads in introns within the 5′UTR of both *trio M* and *trio L* in *Nab2*^{null} heads relative to Control (Figure 2A). Normal splicing patterns are detected across all other *trio* intron-exon junctions. Utilizing a publicly available me-RIP-Seq dataset from *Drosophila* heads (Kan *et al.*, 2021), we bioinformatically identified three m^{6}A sites in the *trio M* 5′UTR (Figure 2A, red lollipops), but none in the *trio L* 5′UTR. These data suggest that Nab2 is required for removal of 5′UTR introns in *trio M* and *trio L* and present the possibility that the removal of the *trio M* 5′UTR could also involve m^{6}A.

To experimentally test this prediction, we first analyzed the *trio M* transcript using reverse transcription PCR (RT-PCR) analysis with primers that detect the *trio M* 5′UTR intron (exon 1-intron 1 and intron 1-exon 2) (Figure 2B, blue and orange primer pairs). This analysis reveals that the *trio M* 5′UTR intron-retaining transcript is enriched in adult heads of *Nab2*^{null} flies as well as in heads lacking *Mettl3,* the catalytic subunit of the methyltransferase complex (Figure 2C) with concomitant reduction or loss of properly spliced *trio M* 5′UTR (exon 1-exon 2) (Figure 2B, red primer pair; see Figure 2C). Primers that detect correctly spliced exon 1-exon 2 *trio M* transcript (Figure 2B, red primer pair) also amplify a ~550 bp band in *Nab2*^{null} heads that is an aberrantly spliced product corresponding to the *trio M* pre-mRNA transcript (Figure 2C). This RT-PCR analysis did not detect the ~4 kb *trio M* 5′UTR intron-retaining transcript, possibly due to the large size of the expected product. To quantitate these results, we performed reverse transcription quantitative PCR (qRT-PCR) analysis, which confirms a significant increase in the levels of the *trio M* 5′UTR intron-retaining transcript in both *Nab2*^{null} and *Mettl3*^{null} heads (Figure 2D). Reciprocal qRT-PCR analysis to quantify the levels of properly spliced *trio M* confirms reduced levels of the properly spliced transcript in *Nab2*^{null} heads and a complete loss of the properly spliced transcript in *Mettl3*^{null} heads (Figure 2E).

Shifting the analysis to the *trio L* 5′UTR intron using primers to detect exon 1-exon 2 confirms the presence of the *trio L* 5′UTR intron-retaining transcript (exon 1-intron 1-exon 2) in *Nab2*^{null} heads and reduced levels of the properly spliced transcript (exon 1-exon 2) (Figure 2F, green primer pair; Figure 2G). In contrast, only properly spliced *trio L* 5′ UTR is detected in heads of flies lacking *Mettl3* (Figure 2G). qRT-PCR analysis confirms increased levels of the *trio L* 5′UTR intron-retaining transcript in *Nab2*^{null}, but not *Mettl3*^{null} heads, as compared with Control (Figure 2H). Reciprocally, qRT-PCR analysis using primers that detect levels of properly spliced *trio L* 5′UTR show reduced transcript levels in *Nab2*^{null} heads and no change in *Mettl3*^{null} heads compared with Control (Figure 2I). Collectively, these data confirm that splicing of the *trio M* and *trio L* 5′UTR introns are both Nab2-dependent, but that only splicing of the *trio M* 5′UTR and not the *trio L* 5′UTR is Mettl3 dependent.

Nab2 regulates levels of Trio M in the *Drosophila* head

The *Drosophila* Trio L protein is most similar to a form of human Trio protein (Trio A) that is enriched in the human brain and nervous system (Portales-Casamar *et al.*, 2006). As illustrated in Figure 3A, Trio L contains a Sec14 domain, nine spectrin repeats, one Src homology 3 (SH3) domain, and two catalytic GEF domains comprised of tandem DH and pleckstrin homology (PH) domains, referred to as GEF1 and GEF2. The *Drosophila* Trio M protein corresponds to the C-terminal end of Trio L, including only the SH3 domain and the GEF2 catalytic domain (Figure 3A).

Based on the finding that Nab2 regulates splicing of the *trio L* and *trio M* 5′UTR introns and that Mettl3 only regulates splicing of the *trio M* 5′UTR intron, we tested whether these intron retention events affect levels of Trio L or Trio M proteins in the fly head. Immunoblotting analysis reveals that Trio L and Trio M are the major isoforms of Trio in Control brains, and that Nab2 loss reduces levels of Trio M but has no apparent effect on Trio L protein levels relative to Control (Figure 3B). Densitometry analysis of the Trio L and Trio M protein levels demonstrates that the decrease in the steady-state level of Trio M protein is statistically significant (Figure 3C). Although loss of *Mettl3* or *Nab2* results in *trio M* 5′UTR intron retention (Figure 2, C–E), only loss of Nab2 causes a concomitant drop in Trio

FIGURE 2: Nab2 and Mettl3 regulate splicing of the *trio* 5′UTR in the *Drosophila* head. (A) RNA-seq reads across the *trio* locus in Control and *Nab2*^{null} fly heads (Jalloh and Lancaster *et al.*, 2023). Boxed insets highlight the sequencing reads from the *trio L* (scale bar = 70 nt) and *trio M* (scale bar = 145 nt) 5′UTR. Red lollipops denote location of mapped m^{6}A sites. (B) Diagram of the *trio M* 5′UTR annotated to show location of color-coded primer pairs. The position of the ATG is also indicated (C) RT-PCR analysis of *trio M* mRNA from Control, *Nab2*^{null}, and *Mettl3*^{null} heads. Properly spliced transcript and intron reattaining transcript bands are indicated. *Rpl32* serves as a control. qRT-PCR analysis detecting levels of (D) intron retaining or (E) properly spliced *trio M* transcript from Control, *Nab2*^{null}, and *Mettl3*^{null} heads, where control is set to 1.0. (F) Diagram of the *trio L* 5′UTR annotated to show location of color-coded primer pairs. (G) RT-PCR analysis of *trio L* mRNA from Control, *Nab2*^{null}, and *Mettl3*^{null} heads. Properly spliced and intron retaining transcript bands are indicated. (H) qRT-PCR analysis detecting levels of intron retaining and (I) properly spliced *trio L* transcript in Control, *Nab2*^{null}, and *Mettl3*^{null} heads. RNA from 25 heads was extracted from each genotype for each biological replicate. At least three biological replicates were performed for each experiment. Significance values are indicated.

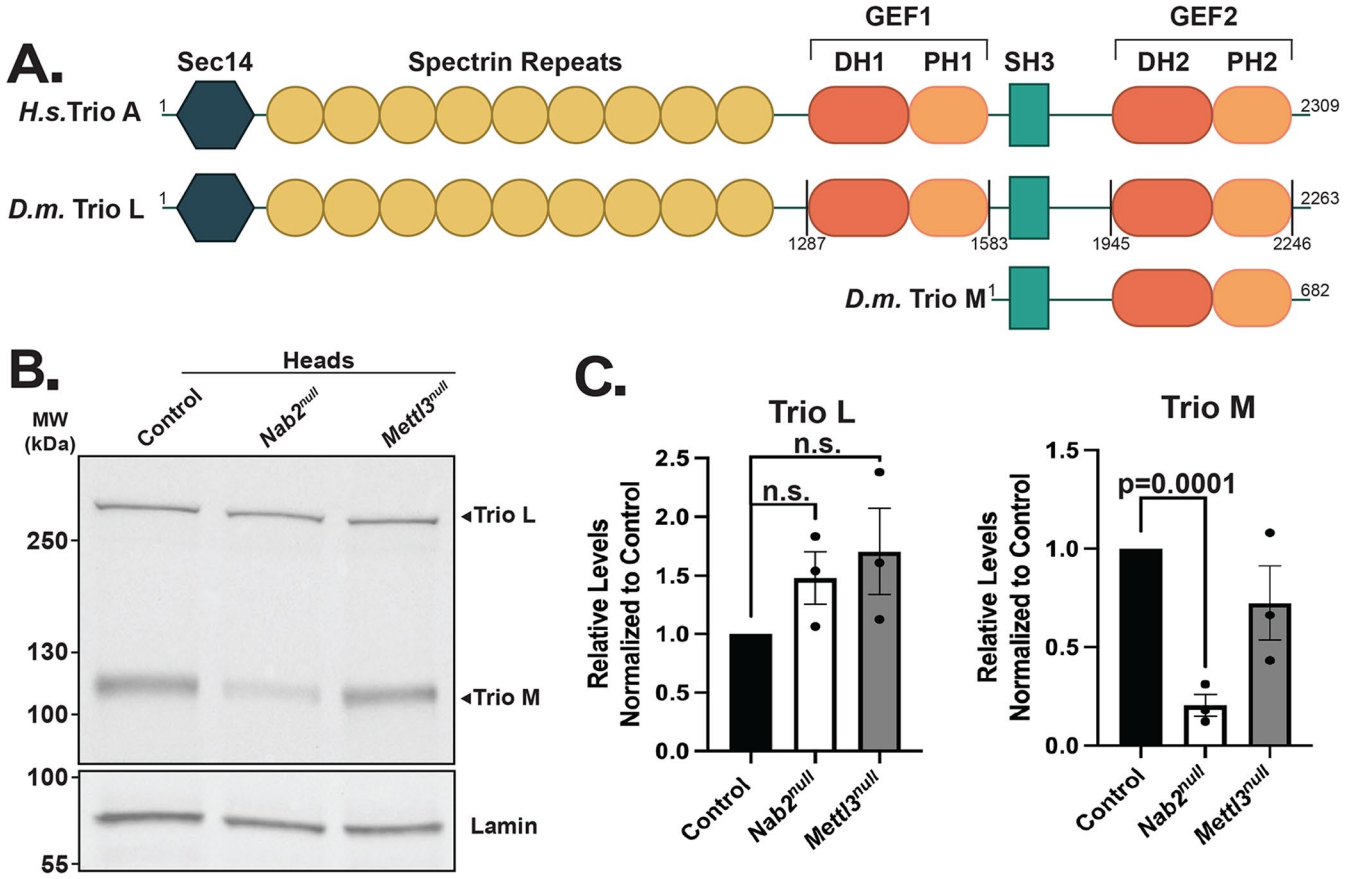

FIGURE 3: Nab2 regulates Trio M protein level in the *Drosophila* head. (A) Schematic of the human (*H.s.*) Trio A and *Drosophila melanogaster* (*D.m.*) Trio L and Trio M proteins. Trio contains a Sec14 domain, nine spectrin repeats, one Src homology 3 (SH3) domain, and two catalytic GEF domains (GEF1 and GEF2), comprised of tandem DH and PH domains. Amino acid lengths are indicated for each Trio protein and the amino acids corresponding to Trio GEF1 and GEF2 are indicated in the schematic for Drosophila Trio L. (B) Immunoblotting analysis of Trio L and Trio M protein levels from Control, *Nab2^{null}*, and *Mettl3^{null}* heads. Lamin serves as a loading Control. Molecular weights in kDa are indicated to the left. (C) Quantification of Trio L (left) and Trio M (right) protein levels in B using Image Lab software. Protein levels are normalized to Control, with the value for Control set to 1.0. Protein from at least 25 heads was extracted from each genotype for each biological replicate. Three biological replicates were performed. Significance values are indicated.

M protein levels (Figure 3, B and C). These results imply an independent effect of Nab2 on postsplicing metabolism of the *trio M* 5′UTR intron retaining mRNA, suggesting additional roles for Nab2 in the regulation of *trio M* translation, trafficking, or turnover.

Trio is altered in the *Nab2^{null}* mushroom body

Previous studies demonstrated that Trio is enriched in the mushroom bodies (Awasaki *et al.*, 2000), which are divided into five lobes per hemisphere (α/α′, β/β′, and γ) that project anteriorly from the dorsally located Kenyon cells (Figure 4A) (Heisenberg, 1998; Roman and Davis, 2001). The α/α′ lobes project dorsally, while the β/β′ and γ lobes project medially, toward the central ellipsoid body (EB) (Figure 4A). As demonstrated previously, loss of Nab2 causes defects in α and β lobe structures, specifically loss or thinning of the α lobes and midline fusion of the β lobe structures (Kelly *et al.*, 2016; Corgiat *et al.*, 2022; Rounds *et al.*, 2022) (Figure 4B). To visualize Trio in these structures, we stained Control brains overexpressing membrane tethered GFP in α/β/γ lobes (*201Y-Gal4, UAS-mcd8::GFP*) with an α-Trio antibody, which recognizes both Trio L and Trio M protein (Awasaki *et al.*, 2000) (Figure 4B). This analysis confirms that Trio is enriched in γ lobes, Kenyon cell bodies, and the calyx as shown by colocalization with GFP, but absent or below the level of detection in α and β lobes (Awasaki *et al.*, 2000) (Figure 4B; Supplemental Figure S1). Intriguingly, Trio accumulates in dysplasic axons near the midline that are not labeled with the *201Y-Gal4* driver (which exclusively drives mcd8::GFP expression in α/β/γ lobes), suggesting these dysplasic axons belong to the β′ lobe (Figure 4B, middle panel, bottom row).

We extended this analysis to explore how loss of Nab2 impacts Trio localization. Trio is lost in the GFP-positive γ lobes of *Nab2^{null}* brains (Figure 4B, bottom row). Given the strong reduction of Trio M protein detected by immunoblotting of *Nab2^{null}* heads (see Figure 2B), this result suggests that Trio M may be the primary isoform of Trio present in mushroom body γ lobes.

To explore the localization of Trio specifically in the α′ and β′ lobe structures, we utilized the Gal4-UAS system to overexpress GFP (*UAS-mcd8::GFP*) using a prime lobe specific Gal4 driver (*Cka^{C305a}-Gal4;* exclusively drives mcd8::GFP expression in α′and β′ lobes) (Figure 4C). As reported previously, Trio is enriched in α′ and β′ axons, and is also detected in γ lobe axons and EB of Control brains (Awasaki *et al.*, 2000) (Figure 4C, top row). *Nab2^{null}* brains show complete loss or thinning of the α′ lobe axons as well as a distinct defasciculation phenotype in the β′ lobe structures (Figure 4C). These morphological phenotypes are accompanied by Trio loss in

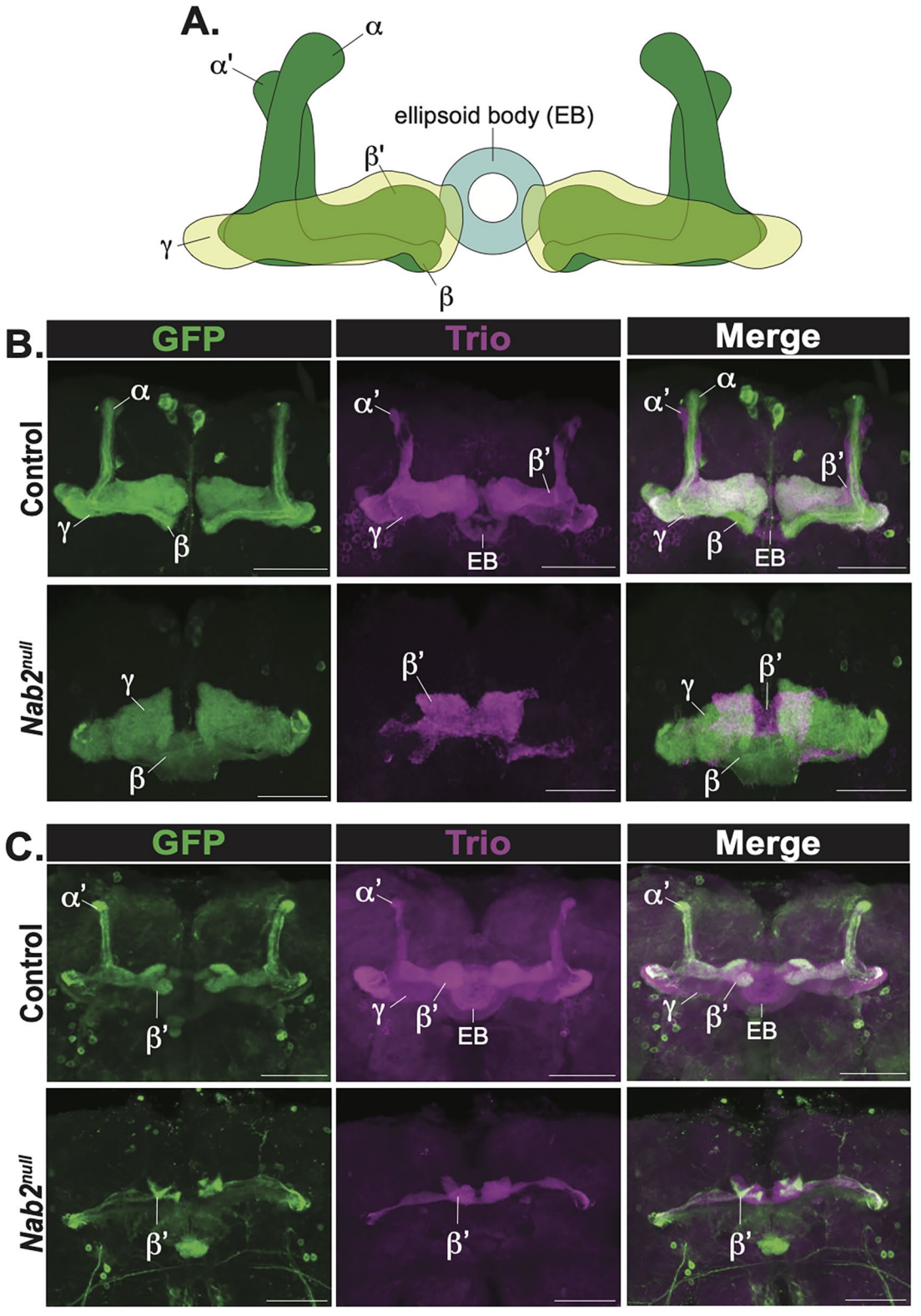

FIGURE 4: Trio is altered in the *Nab2*^{null} mushroom body. (A) Diagram of the adult *Drosophila* mushroom body lobes depicting axons of the medially projecting gamma (γ) neurons, the vertical alpha (α) and alpha prime (α′) neurons, the medially projecting beta (β) and beta prime (β′) neurons, and the EB. (B) Immunofluorescence images of Control (*w-;UAS-mcd8::GFP/201Y-Gal4;;*) and *Nab2*^{null} (*w-;UAS-mcd8::GFP/201Y-Gal4;Nab2*^{null}*;*) mushroom bodies driving *UAS-mcd8::GFP* under the α, β, γ lobe-specific mushroom body *201Y-Gal4* driver. (C) Immunofluorescence images of Control (*w-;UAS-mcd8::GFP/C305a-Gal4;;*) and *Nab2*^{null} (*w-;UAS-mcd8::GFP/C305a-Gal4;Nab2*^{null}*;*) mushroom bodies driving *UAS-mcd8::GFP* under the α′ and β′ lobe-specific mushroom body *C305a-Gal4* driver. False colored panels show fluorescence corresponding to α-GFP (green, mcd8::GFP), α-trio (purple), and merges of the channels. At least 25 brains were analyzed for each genotype. Scale bar = 50 μm.

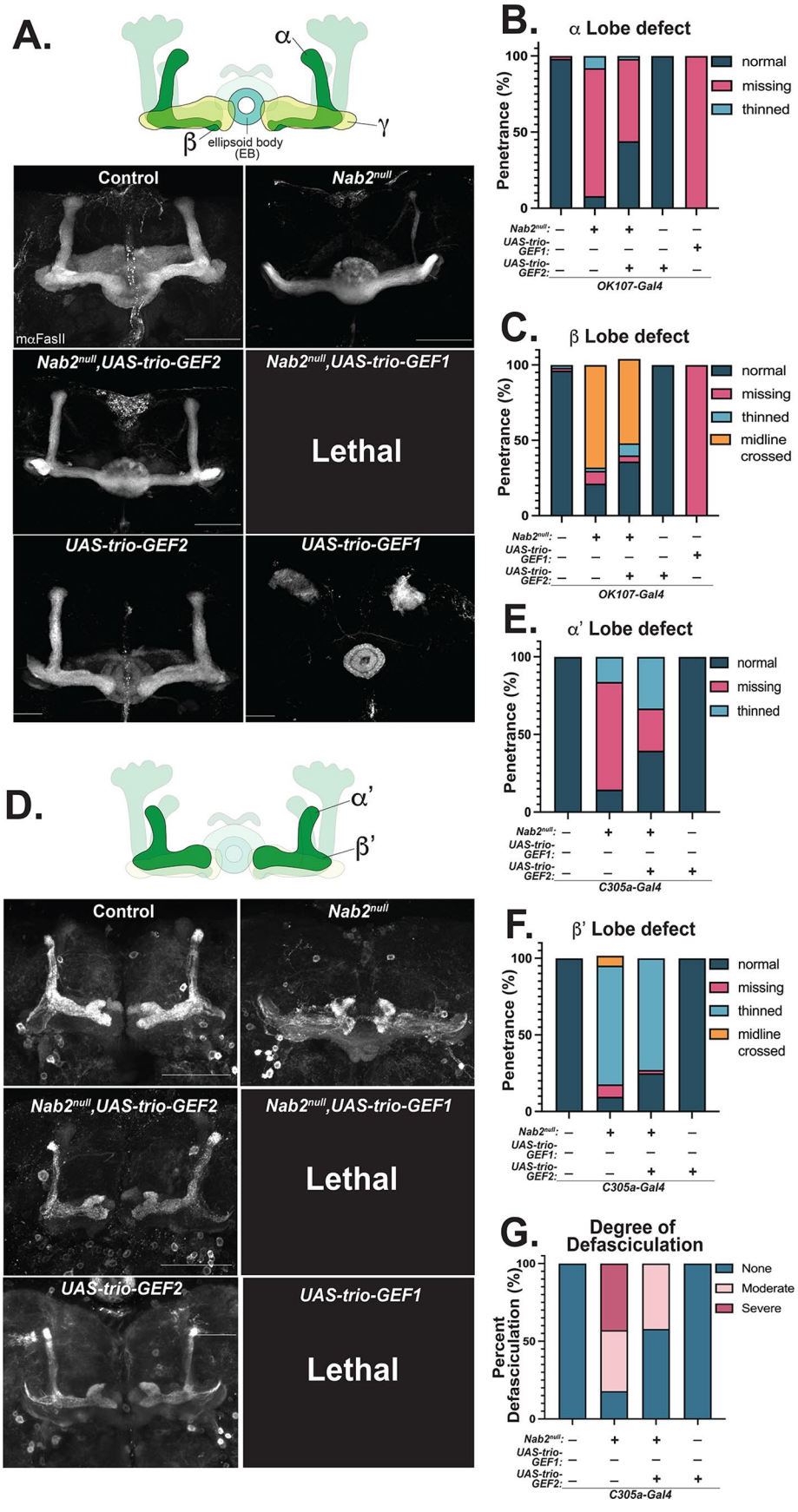

FIGURE 5: Expression of Trio GEF2 rescues α/α′ and β′ defects in *Nab2*^{null} mushroom bodies. (A) Top: Schematic of the *Drosophila* mushroom body with lobes stained by α-Fasciclin II (FasII) highlighted. Bottom: Representative max projections of mushroom bodies of indicated genotypes stained by α-FasII. (B) Quantification of frequency of α lobe defects in each indicated genotype. (C) Quantification of frequency of β lobe defects in indicated genotypes. (D) Top: Schematic of the *Drosophila* mushroom body with lobes overexpressing *mcd8::GFP* under the *C305a-Gal4* driver highlighted. Bottom: Representative max projections of mushroom bodies of indicated genotypes stained with α-GFP. (E) Quantification of frequency of α′ lobe defects in each indicated genotype. (F) Quantification of frequency of β′ lobe defects in indicated genotypes. (G) Quantification of defasciculation phenotype severity in the indicated genotypes. At least 25 brains were analyzed for each genotype. Scale bar = 50 μm.

Nab2^{null}γ lobe axons and EB, and Trio accumulation in the distal portion of β′ lobe axons closest to the brain midline (Figure 4C, middle panel, bottom row).

Expression of Trio GEF2 rescues α/α′ and β′ defects in *Nab2*^{null} mushroom bodies

The reduced level of Trio M protein in *Nab2*^{null} heads (Figure 3B) raises the possibility that an imbalance in the relative dose of Trio-GEF1 and Trio-GEF2 activities contributes to mushroom body morphology defects observed in *Nab2*^{null} flies (Kelly *et al.*, 2016). This model is based on the established role of the Trio protein in patterning of axons in the mushroom body (Awasaki *et al.*, 2000), and predicts that loss of Trio M lowers Trio-GEF2 activity within specific mushroom body lobes.

To test this model, transgenes encoding specifically the Trio-GEF1 (*UAS-Trio*-GEF1; Figure 3A, AAs 1287–1583 tagged at the 3′end with eight copies of the tag MYC) or Trio-GEF2 domain (*UAS-Trio-GEF2*; Figure 3A, AAs 1945–2246 tagged at the 3′end with eight copies of the tag MYC) (Awasaki *et al.*, 2000; Newsome *et al.*, 2000), were expressed in all mushroom body lobes of *Nab2*^{null} brains using the *OK107-Gal4* driver. As previously reported (Kelly *et al.*, 2016; Bienkowski *et al.*, 2017; Corgiat *et al.*, 2021; Corgiat *et al.*, 2022; Rounds *et al.*, 2022) and shown in Figures 5, A–C, *Nab2*^{null} mutant brains have highly penetrant defects in the structure of the mushroom body α lobes (missing or thinned) and β lobes (missing, thinned, or midline crossed) as detected by α-FasII staining, which specifically recognizes the α, β and weakly the γ lobes (Crittenden *et al.*, 1998). Transgenic expression of Trio-GEF2 alone has no effect on mushroom body structure in a control

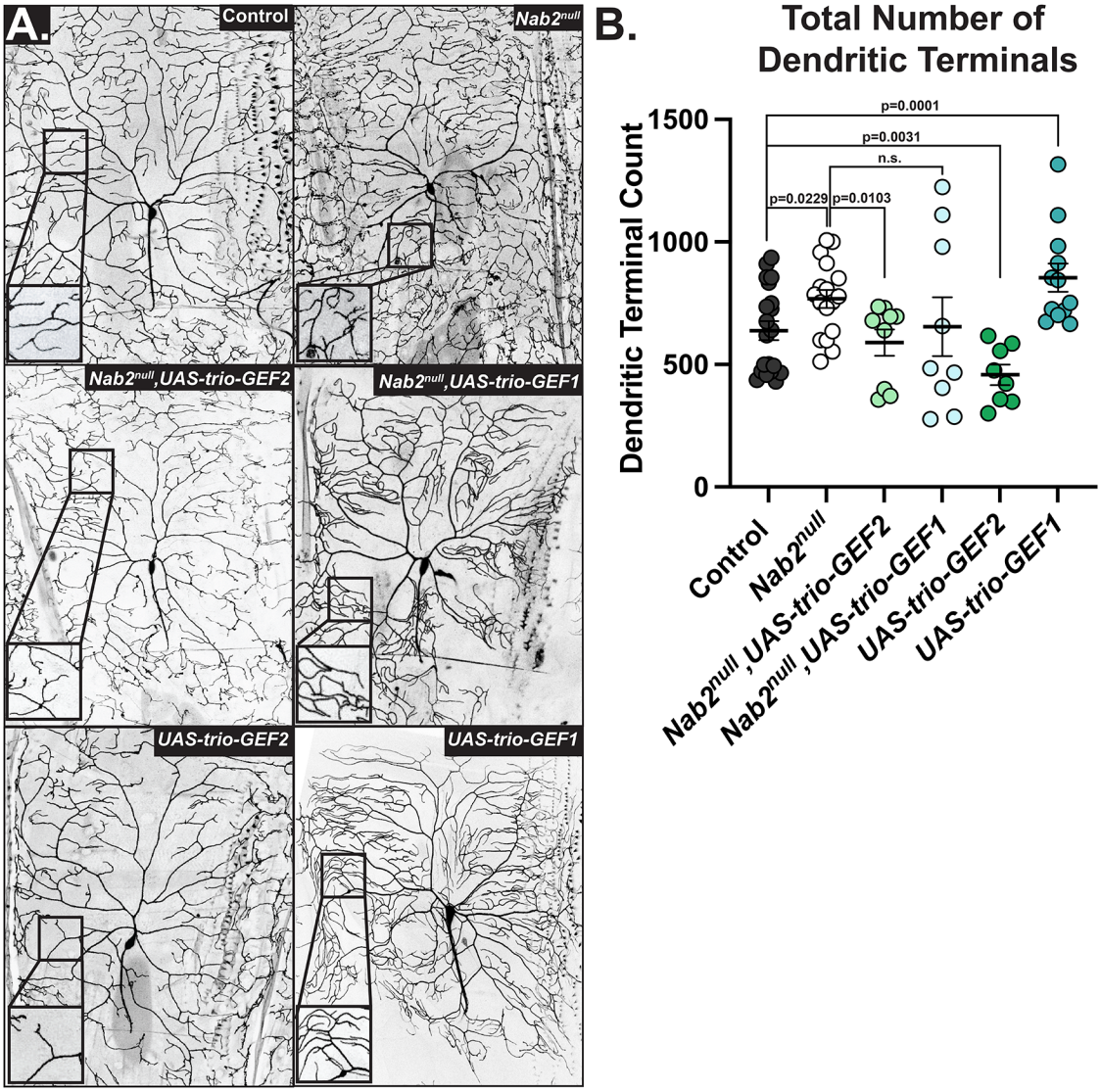

FIGURE 6: Expression of Trio GEF2 rescues *Nab2*^{null} dendritic arborization defects in class IV ddaC sensory neurons. (A) Maximum intensity projections of *Drosophila* class IV ddaC neurons from Control, *Nab2*^{null}, *Nab2*^{null} *UAS-Trio-GEF2, Nab2*^{null} *UAS-Trio-GEF1, UAS-Trio GEF2, and UAS-Trio-GEF1* L3 larvae. Inset black boxes show high magnification views of dendritic arbors. (B) Quantification of total number of dendritic terminals for each genotype. At least eight neurons were measured for each genotype. Significance values are indicated.

background. Intriguingly, transgenic expression of Trio-GEF2 does not rescue *Nab2*^{null} β lobe defects, but significantly suppresses *Nab2*^{null} α lobe defects (Figure 5, A–C). In contrast, mushroom body expression of Trio-GEF1 in control brains causes complete loss of axonal projection from the Kenyon cells (no lobe structures were detected in any of the brains analyzed; $n = 25$) and is completely lethal in a *Nab2*^{null} background (Figure 5, A–C). Thus, Nab2 loss sensitizes mushroom body axons to the dose of Trio GEF domains such that expression of Trio-GEF2 rescues α lobe axons and expression of extra Trio-GEF1 is lethal to the animal; neither effect is observed in Control brains, indicative of a tight link between Nab2 and Trio GEF dosage in the developing mushroom body.

Given the enrichment of Trio protein in the α′ and β′ lobes (see Figure 4B), we also tested whether transgenic expression of the Trio GEF1 or GEF2 domain could autonomously rescue *Nab2*^{null} α′ or β′ lobe morphology as visualized with the *Cka*^{C305a}*-Gal4* driver (with *UAS-mcd8::GFP*). As with Trio-GEF1 or Trio-GEF2 expression in the α, β, and γ lobes using the *201Y-Gal4* driver, expression of Trio-GEF2 alone has no effect on α′ and β′ lobe morphology in Control brains but rescues *Nab2*^{null} defects in α′ lobe structure and strongly reduces β′ lobe defasciculation (Figure 5, D–G). Expression of Trio-GEF1 in α′ and β′ lobes has the inverse effect of late larval lethality in both Control and *Nab2*^{null} animals (Figure 5D). These data are consistent with a model in which Nab2 acts through Trio-GEF2 to guide axon projection and fasciculation in the α′ and β′ lobes.

Expression of Trio GEF2 rescues *Nab2*^{null} dendritic arborization defects in class IV ddaC sensory neurons

Nab2 normally restricts branching of sensory dendrites in larval class IV ddaC neurons in body wall neurons (Corgiat *et al.*, 2022). Significantly, Trio-GEF1 promotes and Trio-GEF2 restricts branching of dendrites from these same class IV ddaC neurons (Figure 6, A and B) (Iyer *et al.*, 2012). Thus, we reasoned that an imbalance of Trio-GEF1 and Trio-GEF2 activities in *Nab2*^{null} ddaC neurons might contribute

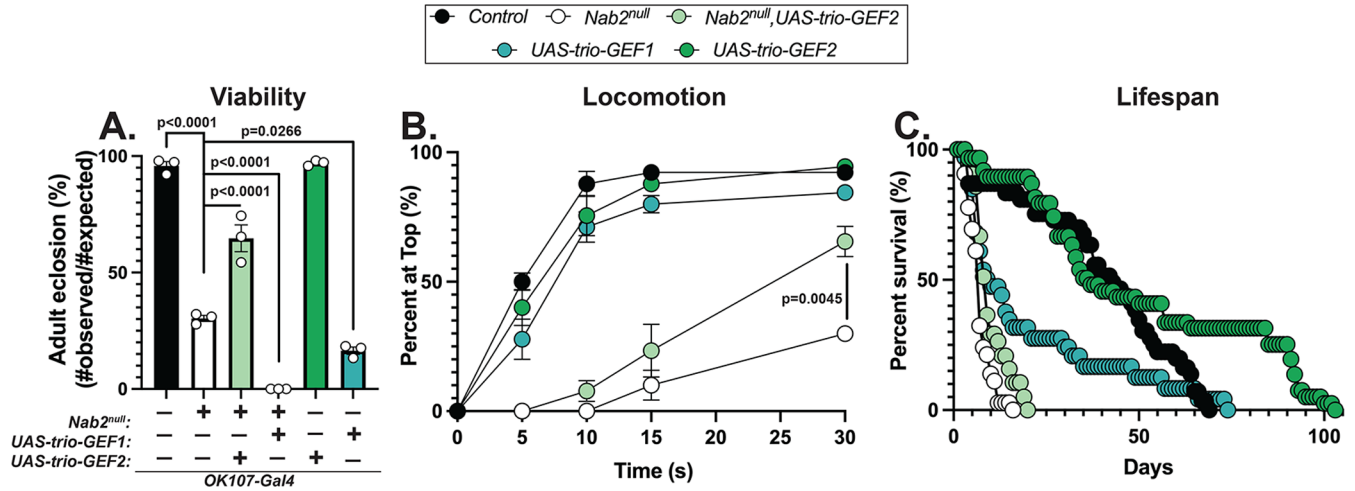

FIGURE 7: Expression of Trio GEF2 rescues *Nab2*^{null} defects in viability and locomotion. (A) Percent of Control, *Nab2*^{null}, *Nab2*^{null} *UAS-Trio-GEF2, UAS-Trio GEF2,* or *UAS-Trio-GEF1* that eclose as viable adults (calculated as #observed/#expected) using the *OK107-Gal4* mushroom body driver. (B) Negative geotaxis of age-matched adult flies of indicated genotypes over time in seconds (s). (C) Survival of age matched adult flies of the indicated genotypes over time in days. At least three biological replicated were tested for each genotype. Significance values are indicated.

to dendritic defects. To test this model, we employed a *pickpocket* (*ppk*)*-Gal4,UAS-mcd8::GFP* system to visualize class IV ddaC cell bodies and dendritic trees. As observed previously, loss of Nab2 (Corgiat *et al.*, 2022) or transgenic expression of Trio-GEF1 (Iyer *et al.*, 2012) individually increases dendritic branch complexity, while transgenic expression of Trio-GEF2 reduces dendritic branch complexity (Iyer *et al.*, 2012) (Figure 6, A and B). Significantly, combining Nab2 loss (*Nab2*^{null}) with ddaC-specific expression of Trio-GEF2 rescues overarborization normally observed in *Nab2*^{null} larvae (Figure 6, A and B). Intriguingly, transgenic expression of Trio-GEF1 in *Nab2*^{null} larvae causes an increase the variance between arborization phenotypes among the neurons analyzed (Figure 6B). Together, these data indicate that loss of Trio-GEF2 in *Nab2*^{null} larvae likely contributes to *Nab2*^{null} ddaC overarborization defects.

Expression of Trio GEF2 rescues *Nab2*^{null} defects in viability and locomotion

Given the genetic interactions between the *UAS-Trio-GEF1* and *UAS-Trio-GEF2* transgenes and *Nab2*, we assessed whether transgenic expression of these distinct Trio GEF domains in the mushroom body (*OK107-Gal4, UAS-Trio-GEF1* or *UAS-Trio-GEF2*) affects the organismal phenotypes of viability, adult locomotion, and lifespan. Confirming our previous findings (Pak *et al.*, 2011), we detected severe reductions in viability, adult locomotion, and lifespan in *Nab2*^{null} flies compared with Control (Figure 7, A–C). As previously noted, expression of Trio-GEF1 in mushroom bodies is lethal at late larval stages (Figure 7A). In contrast, transgenic expression of Trio-GEF2 in mushroom bodies strongly suppresses *Nab2*^{null} defects in viability and suppresses defects in adult locomotion but does not significantly alter lifespan (Figure 7, A–C), indicating that a deficit in Trio-GEF2-regulated cytoskeletal dynamics within *OK107*-expressing brain neurons contributes to developmental and postdevelopmental defects in *Drosophila* lacking Nab2.

DISCUSSION

Here, we identify a role for the *Drosophila* Nab2 RBP and Mettl3 m^{6}A methyltransferase in regulating the *trio* mRNA, which encodes a conserved RhoGEF protein that is altered in human intellectual disability and regulates axon guidance and dendritic arborization through two GEF domains that individually control the cytoskeletal regulators Rac and RhoA/Rho1 (Debant *et al.*, 1996; Bellanger *et al.*, 1998a; Bellanger *et al.*, 1998b; Bateman and Van Vactor, 2001; Jaffe and Hall, 2005; Briancon-Marjollet *et al.*, 2008; Iyer *et al.*, 2012; Bircher and Koleske, 2021). The data presented provide strong evidence that the *trio* transcript is a key downstream target of Nab2 in neurons based on an m^{6}A- and Nab2-dependent splicing event and identifies specific effects of each Trio GEF domain within axons and dendrites that develop from neurons lacking Nab2. The results of this study combine with our previous work (Corgiat *et al.*, 2022; Jalloh and Lancaster *et al.*, 2023) to support a model in which Nab2 regulates transcripts that encode key regulators of neurodevelopment, including the conserved GEF, Trio. In the broader context, the phenotypic consequences of loss of an RBP result from the collective changes to numerous target transcripts, and defining the mechanistic basis of these phenotypes requires systematic analysis of how individual targets, such as *trio*, are impacted. In the case of Nab2, evidence now supports both m^{6}A-dependent and independent roles in *trio* mRNA splicing as well as potential effects on downstream processing such as cytoplasmic metabolism of *trio* mRNA. Taken together, these findings support a model where RBPs such as Nab2/ZC3H14 regulate a collection of target transcripts, potentially through multiple mechanisms, that all contribute to downstream phenotypes.

Previous work illustrating broad rescue of *Nab2*^{null} phenotypes by Mettl3 heterozygosity (Jalloh and Lancaster *et al.*, 2023) suggested that other regulators of m^{6}A-modified transcripts could also contribute to *Nab2*^{null} defects in viability, adult locomotion, and lifespan. Here, we demonstrate that loss of nuclear or cytoplasmic m^{6}A reader function rescues some, but not all, organismal phenotypes associated with loss of Nab2 (Figure 1). Homozygous loss of the nuclear m^{6}A reader YT521-B suppresses *Nab2*^{null} defects in viability, but not locomotion or lifespan, whereas heterozygous loss of the cytoplasmic m^{6}A reader Ythdf dominantly suppresses *Nab2*^{null} defects in locomotion, but not viability or lifespan. Collectively, these data suggest that mRNA targets of Nab2 responsible for these behavioral phenotypes may be differentially regulated between cell types and in an m^{6}A-dependent manner. For instance, Nab2-regulated transcripts encoding proteins that govern

Drosophila viability could rely more heavily on nuclear m^{6}A regulatory mechanisms, such as splicing or export. On the other hand, Nab2-regulated transcripts encoding proteins that govern *Drosophila* negative geotaxis could more heavily require cytoplasmic m^{6}A regulatory mechanisms, such as translation or stability. Moreover, the inability of *YT521-B* or *Ythdf* loss to rescue *Nab2^{null}* defects in lifespan suggests that Nab2-regulated transcripts that govern lifespan may not by modified by m^{6}A, or that Nab2 plays m^{6}A-independent roles in regulating transcripts critical to control lifespan.

Previous studies demonstrated that loss of m^{6}A regulatory proteins disrupts axon projection in the *Drosophila* mushroom body (Kan *et al.*, 2021; Worpenberg *et al.*, 2021). Although *Mettl3* heterozygosity broadly rescues *Nab2^{null}* behavioral defects (Jalloh and Lancaster *et al.*, 2023), a decrease in Mettl3 does not dominantly suppress mushroom body morphology defects (Supplemental Figure S2). This finding suggests that Mettl3 heterozygosity is insufficient to reduce m^{6}A methylation on Nab2-target transcripts to a degree necessary for rescue of axonal projection defects. Given the ability of m^{6}A writer and reader alleles to broadly rescue *Nab2^{null}* phenotypes, future studies will aim to further define the relationship between m^{6}A machinery and Nab2 in relation to regulation of *Drosophila* mushroom body morphology. Moreover, a genome-wide approach to assess transcriptomic changes in m^{6}A in *Nab2^{null}* flies will help delineate the neuronal, Nab2-regulated transcripts that exhibit changes in m^{6}A methylation.

A number of *trio* transcript variants exist in the *Drosophila* brain (Awasaki *et al.*, 2000). Here, we demonstrate that both Nab2 and Mettl3 are required for proper splicing of the 5′UTR intron of *trio M*. On the other hand, splicing of the 5′UTR intron of *trio L* is dependent on Nab2 but not Mettl3. These data align with previously published RNA-seq data from *Nab2^{null} Drosophila* heads (Jalloh and Lancaster *et al.*, 2023), as well as a publicly available mi-CLIP-seq dataset that mapped m^{6}A sites in the *trio M* 5′UTR intron, but not in the *trio L* 5′UTR intron (Kan *et al.*, 2021). Notably, our data reveal that disruptions in splicing of the *trio* 5′UTR due to loss of Nab2 or Mettl3 do not correspond with perturbations in steady-state levels of Trio L and Trio M proteins. These results show that the intron retention event in the 5′UTR of *trio M* is associated with a significant reduction in the level of Trio M protein in the *Nab2^{null}* fly head. Surprisingly, the steady-state level of Trio M protein is unaffected in *Mettl3^{null}* heads even though *trio* 5′UTR intron retention is comparable to the levels observed in *Nab2^{null}* heads. These data imply that Nab2 may regulate *trio M* protein levels in a manner independent of *trio M* 5′UTR splicing. However, given previously defined roles for Nab2 as a negative regulator of m^{6}A methylation (Jalloh and Lancaster *et al.*, 2023), this observation more likely suggests that excess m^{6}A on the *trio M* pre-mRNA upon loss of Nab2 may disrupt subsequent translation, trafficking, or stability. In contrast, retention of the *trio L* 5′UTR intron that occurs upon loss of Nab2 does not affect the steady-state level of the Trio L protein, suggesting this intron retention event may not disrupt translation. Alternatively, the remaining level of the properly spliced *trio L* in *Nab2^{null}* heads may be sufficient to maintain the steady-state level of Trio L protein. Further studies expanding to additional coregulated Nab2 and Mettl3 targets will be required to define how these factors regulate posttranscriptional events.

Given that Nab2 regulates splicing and downstream processing of numerous neuronally-enriched mRNAs (Jalloh and Lancaster *et al.*, 2023), morphological defects observed in *Nab2^{null}* mushroom bodies are likely due to collective processing defects that affect multiple RNAs critical for axon development. Our results support a model where loss of Trio M, and therefore GEF2 function, contributes to morphological defects in mushroom bodies of *Nab2^{null}* flies. Previous studies demonstrated that Trio is a critical regulator of mushroom body morphology and Trio is enriched in the α′, β′, and γ lobes, but is virtually absent in the α and β lobes (Awasaki *et al.*, 2000). We confirm these findings and further demonstrate that upon loss of Nab2, Trio levels are depleted in the γ lobes. Despite the established functions of Trio in regulating γ lobe formation (Awasaki *et al.*, 2000), γ lobe defects are not detected upon loss of Nab2 (Kelly *et al.*, 2016). Given that Trio M is the only isoform of Trio depleted in *Nab2^{null}* brains (Figure 3B) and γ lobes show no defects (Figure 5A), this finding suggests that Trio L, and therefore GEF1 function, is responsible for patterning γ lobe axons in the developing brain.

Studies of axon pathfinding mechanisms in the mushroom body demonstrate that the α′ and β′ lobes guide development of the α and β lobes (Fushima and Tsujimura, 2007). Given that Trio is enriched in the α′/β′/γ lobes of the mushroom body, our data suggest that loss of Trio M, and therefore GEF2 levels, in α′/β′ lobes contributes to *Nab2^{null}* α/β lobe defects. We demonstrate that transgenic expression of Trio-GEF2 in α′/β′ lobes (*C305a-Gal4*) of *Nab2^{null}* mushroom bodies rescues α′ lobe defects and β′ lobe defasciculation phenotypes in a cell autonomous manner (Figure 5). Moreover, expression of Trio-GEF2 in all mushroom body lobes (*OK107-Gal4*) rescues *Nab2^{null}* α lobe defects; however, whether this rescue occurs in a cell autonomous manner remains unknown (Figure 5). Collectively, these data demonstrate that Trio-GEF2 rescue is limited to some mushroom body lobes (α, α′, β′) and not others (β), implying that Trio-GEF2 is required for projection of only some *Nab2^{null}* axons. In this regard, misprojection defects in *Nab2^{null}* β axons are not rescued by multiple genetic manipulations that rescue α axon defects (e.g., by transgenic expression of Trio-GEF2 [this study] or by single copy alleles of *fmr1*, *Atx2*, or PCP components [Kelly *et al.*, 2016; Bienkowski *et al.*, 2017; Rounds *et al.*, 2021; Corgiat *et al.*, 2022]). These findings imply specific roles for Nab2 in these two types of Kenyon cell projections and suggest that Nab2 regulates different mRNAs to govern development of distinct mushroom body lobes.

Previous studies established that the Trio-GEF1 domain acts primarily through activation of Rac1 to promote axon outgrowth and pathfinding, while Trio-GEF2 acts primarily through RhoA/Rho1 to restrict neurite outgrowth (Leeuwen *et al.*, 1997; Iyer *et al.*, 2012; Bircher and Koleske, 2021). Given that loss of Nab2 disrupts the ratio of GEF1 and GEF2 in *Drosophila* heads by decreasing the level of Trio M but not Trio L, we hypothesized that expression of the GEF1 effector, Rac1, in mushroom body neurons would exacerbate *Nab2^{null}* phenotypic and morphological defects, whereas expression of the GEF2 effector, RhoA/Rho1, would rescue these same defects. Intriguingly, we observed that expression of either Rac1 or RhoA/Rho1 in the absence of Nab2 in Trio-enriched mushroom body neurons is lethal (Supplemental Figure S3). These data suggest that further expression of Rac1 in *Nab2^{null}* flies in which GEF1 levels, and therefore likely Rac1 activation, dominates is detrimental to nervous system development and the lethality induced by expression of RhoA/Rho1 upon loss of Nab2, indicates that Trio-GEF2 may act via other unknown effectors to govern mushroom body development. On the other hand, alternative RhoGEFs may compensate for the loss of Trio M protein in the mushroom body thereby leading to the lethality of *Nab2^{null}* animals transgenically expressing Rac1 or RhoA/Rho1. In sum, further studies are required to elucidate how loss of Nab2 alters Rac1 and RhoA/Rho1 activity in the *Drosophila* brain.

Nab2 and Trio have established roles in sculpting dendritic arborization of class IV ddaC neurons in the *Drosophila* PNS (Iyer *et al.*, 2012; Corgiat *et al.*, 2022). Here, we demonstrate that transgenic expression of the Trio-GEF2 domain rescues overarborization defects in *Nab2*^{null} class IV ddaC neurons. In line with previous studies (Iyer *et al.*, 2012), we validate that transgenic expression of Trio-GEF1 in class IV ddaC neurons causes dramatic overarborization defects, while transgenic expression of Trio-GEF2 causes underarborization defects compared with control animals. Interestingly, we also demonstrate that expression of Trio-GEF1 in class IV ddaC neurons of *Nab2*^{null} flies results in a wide range of arborization phenotypes. Very few of these animals survive to the wandering third instar larval stage and no animals survive to adulthood. Given these observations, disruption of Nab2-regulated mRNAs in these neurons as well as overactivation of Rac1 by GEF1 may severely disrupt ddaC development such that arborization defects are highly variable from animal-to-animal. Overall, these data support a role for Trio M, and therefore GEF2 loss, in contributing to the established overarborization defects in *Nab2*^{null} class IV ddaC neurons (Corgiat *et al.*, 2022).

In aggregate, these data reveal a role for Nab2 and Mettl3 in regulating splicing and protein levels of the RhoGEF Trio to support proper nervous system development. Genetic interactions between the m^{6}A machinery and Nab2 support a role for Nab2 in the regulation of m^{6}A methylation. We show for the first time that loss of Trio M, and therefore GEF2 levels, in *Nab2*^{null} flies contributes to several *Nab2*^{null} defects, including neuronal defects, such as mushroom body morphology and class IV ddaC arborization. Moreover, we demonstrate that transgenic expression of Trio-GEF2 broadly rescues *Nab2*^{null} viability and adult locomotion. This regulatory relationship between Nab2 and Trio-GEF2 could be cell autonomous, but further experiments are required determine the nature of this interaction. Given that mutations in human *ZC3H14* and *TRIO* are both linked to intellectual disabilities (Pak *et al.*, 2011; Ba *et al.*, 2016), dysregulation of Trio function in neurons is one potential mechanism to explain axonal and dendritic phenotypes observed in *Nab2*^{null} *Drosophila* (Pak *et al.*, 2011; Kelly *et al.*, 2016; Bienkowski *et al.*, 2017; Corgiat *et al.*, 2021; Corgiat *et al.*, 2022; Jalloh and Lancaster *et al.*, 2023) and *Zc3h14* mutant mice (Jones *et al.*, 2020), as well as the cognitive defect observed in human patients lacking ZC3H14 (Pak *et al.*, 2011).

MATERIALS AND METHODS

Request a protocol through *Bio-protocol*.

Resources table

Reagent or resource	Source	Identifier
Antibodies		
Mouse monoclonal 9.4A anti-Trio	University of Iowa Developmental Studies Hybridoma Bank	RRID:AB_528494
Mouse monoclonal ADL101 anti-Lamin	University of Iowa Developmental Studies Hybridoma Bank	RRID:AB_528332
Mouse monoclonal 1D4 anti-Fasciclin II	University of Iowa Developmental Studies Hybridoma Bank	RRID: AB_528235
Rabbit Polyclonal Anti-Green Fluorescent Protein (GFP)	Thermo Fisher Scientific	Catalogue no. A-11122
Alexa Fluor 488 AffiniPure Polyclonal Goat Anti-rabbit IgG	Jackson ImmunoResearch Laboratories	RRID: AB_2338046
Cy3 AffiniPure Polyclonal Goat Anti-Mouse IgG	Jackson ImmunoResearch Laboratories	RRID: AB_2338690
Chemicals, peptides, and recombinant proteins		
TRIzol reagent	Invitrogen	Catalogue no. 15596018
1-Bromo-3-chloropropane	Scientific Laboratory Supplies	Catalogue no. B9673
2-propanol/isopropanol	Thermo Fisher Scientific	Catalogue no. A416-1
Ethanol 200 proof	Thermo Fisher Scientific	Catalogue no. 04-355-233
Diethyl pyrocarbonate (DEPC)	Sigma-Aldrich	Catalogue no. D5758
Agarose LE, Quick Dissolve	Genesee Scientific	Catalogue no. 20-102QD
Red Safe	iNtRON Biotechnology	Catalogue no. 21141
NaCl	Sigma-Aldrich	Catalogue no. S7653
KCl	Sigma-Aldrich	Catalogue no. P3911
$ZnCl_2$	Sigma-Aldrich	Catalogue no. 208086
Polysorbate 20 (Tween 20)	Fisher Bioreagents	Catalogue no. BP-337-500
Triton X-100	Sigma-Aldrich	Catalogue no. T8787
Tris Base Ultrapure	USBiological Life Sciences	Catalogue no. T8600
Sodium Dodecyl Sulfate	Fisher Bioreagents	Catalogue no.YBP166500

(*Continues*)

Reagent or resource	Source	Identifier
Sodium deoxycholate	Thermo Fisher Scientific	Catalogue no. 89905
NP-40	Thermo Fisher Scientific	Catalogue no. 85124
Dithiothreitol (DTT)	Thermo Fisher Scientific	Catalogue no. R0861
Bromophenol Blue	Thermo Fisher Scientific Chemicals	Catalogue no. A18469-18
Glycerol	USBiological Life Sciences	Catalogue no. G8145
RNaseOUT	Invitrogen	Catalogue no. 10777019
p-Coumaric acid	Sigma-Aldrich	Catalogue no. C9008
Luminol	Sigma-Aldrich	Catalogue no.A8511
Acetic Acid, Glacial	Thermo Fisher Scientific	Catalogue no. A38-212
EDTA	USBiological Life Sciences	Catalogue no. E2210
Paraformaldehyde	Electron Microscopy Sciences	Catalogue no. 15713
VECTASHEILD mounting medium	Vector Laboratories Inc.	REF#H-1000
Normal Goat Serum	Jackson ImmunoResearch Laboratories	RRID:AB_2336990
Diethyl Ether Anhydrous (stabilized with BHT)	Tokyo Chemical Industry (TCI) America	Catalogue no. D3497
Halocarbon oil 27	Sigma-Aldrich	Catalogue no. H8773
Critical commercial assays		
DNase I, Amplification Grade	Invitrogen	Catalogue no. 18068015
M-MLV Reverse Transcriptase	Invitrogen	Catalogue no. 28025013
Taq DNA Polymerase (1000U)	Qiagen	Catalogue no. 201205
QuantiTect SYBR Green PCR Kit	Qiagen	Catalogue no. 204145
MicroAmp Fast Optical 96-Well Reaction Plate with Barcode, 0.1 ml	Applied Biosystems	Catalogue no. 4346906
MicroAmp Optical Adhesive Film	Applied Biosystems	Catalogue no. 4311971
4–20% Mini-PROTEAN TGX Stain-Free™ Protein Gels	Bio-Rad	Catalogue no. 4568093
Nitrocellulose Membrane, 0.2 µm	Bio-Rad	Catalogue no. 1620112
iScript Reverse Transcriptase Supermix	Bio-Rad	Catalogue no. 1708841
Phusion High Fidelity PCR	Thermo Fisher Scientific	Catalogue no. F530S
Pierce BCA Protein Assay Kit	Thermo Fisher Scientific	Catalogue no. 23225
SuperFrost Plus slides	Thermo Fisher Scientific	Catalogue no. 12-550-15
Il90p-Experimental models: Organisms/Strains		
D. melanogaster: w-;;Nab2^{pex41} (Control);	(Pak *et al.*, 2011)	N/A
D. melanogaster: w-;;Nab2^{ex3} (*Nab2^{null}*); (Zygotic loss of Nab2)	(Pak *et al.*, 2011)	N/A
D. melanogaster: w-;;Mettl3^{null};	(Lence *et al.*, 2016)	N/A
D. melanogaster:YT521-B$^{\Delta N}$	(Lence *et al.*, 2016)	N/A
D. melanogaster: Ythdf$^{\Delta YTH}$ (Ythdf^{0})	(Worpenberg *et al.*, 2021)	N/A
D. melanogaster:w^{1118};;Df(3R)BSC655 (ythdf deficiency)	Bloomington Drosophila Stock Company	BDSC:26507
D. melanogaster: y^{1}w^{67c23};UAS-mcd8::GFP, 201Y-Gal4;;	Bloomington Drosophila Stock Company	BDSC:64296
D. melanogaster:w;Cka^{c305a}-Gal4*	Bloomington Drosophila Stock Company	BDSC:30829
D. melanogaster: y^{1}w;UAS-mcd8::GFP;;*	Bloomington Drosophila Stock Company	BDSC:5137
D. melanogaster: w;;;OK107-Gal4*	Bloomington Drosophila Stock Company	BDSC:854
D. melanogaster:y^{1}w:UAS-trio-GEF1-myc* (Trio-GEF1 domain; AAs 1287-1583 tagged at the 3′end with eight copies of the tag MYC)	Bloomington Drosophila Stock Company	BDSC:9133

(*Continues*)

Reagent or resource	Source	Identifier
D. melanogaster: y[1]w:UAS-trio-GEF2-myc* (Trio-GEF2 domain; AAs 1945-2246 tagged at the 3′end with eight copies of the tag MYC)	Bloomington Drosophila Stock Company	BDSC:9134
D. melanogaster:w;;ppk-Gal4*	Bloomington Drosophila Stock Company	BSDC:32079
D. melanogaster:w;UAS-Rac1*	Bloomington Drosophila Stock Company	BSDC:6293
D. melanogaster:w;UAS-Rho1*	Bloomington Drosophila Stock Company	BSDC:58819
Oligonucleotides		
RT-PCR *trio L* Forward: AACAAAACAGAGAGCGCCC	This study	N/A
RT-PCR *trio L* Reverse: GATGGGCACTGCAGCATAA	This study	N/A
qRT-PCR *trio L* Intron Retention Forward: 5′-TTAGCCCGCGTCAAGTC-3′	This study	N/A
qRT-PCR *trio L* Intron Retention Reverse: 5′-CTGCTTGTGCCACCAAAT-3′	This study	N/A
qRT-PCR *trio L* Properly Spliced Forward: 5′-GTTGTGTTGACAAAAGAGTG-3′	This study	N/A
qRT-PCR *trio L* Properly Spliced Reverse: 5′-GATGGGCACTGCAGCATAA-3′	This study	N/A
RT-PCR *trio M* Intron Retention (1) Forward: 5′-CAGCAGTCTCTTCTTCACTAA-3′	This study	N/A
RT-PCR *trio M* Intron Retention (1) Reverse: 5′-ACTCGGATTGTTGTTTCACTTT-3′	This study	N/A
RT-PCR *trio M* Intron Retention (2) Forward: 5′-GACTGCGCAAACATAGCATTA-3′	This study	N/A
RT-PCR *trio M* Intron Retention (2) Reverse: 5′-ATCCGCTCGTTGAGAAACT-3′	This study	N/A
RT-PCR *trio M* Properly Spliced Forward: 5′-CGCTAAAGAGGAGCGCAATA-3′	This study	N/A
RT-PCR *trio M* Properly Spliced Reverse: 5′-CTTCTTAACACTCTTCATGATTCG-3′	This study	N/A
qRT-PCR *trio M* Intron Retention Forward: 5′-TTGAGTGAACCCGCTAAAG-3′	This study	N/A
qRT-PCR *trio M* Intron Retention Reverse: 5′-CTTTGGAGTGCTTGTTCTTATC-3′	This study	N/A
qRT-PCR *trio M* Properly Spliced Forward: CGTCCATAAATTGAGTCGGAGAAC	This study	N/A
qRT-PCR *trio M* Properly Spliced Reverse: 5′-CTTCTTAACACTCTTCATGATTCG-3′	This study	N/A
RT-PCR and qRT-PCR *rpl32* Forward: AAGATGACCATCCGCCCAGCATAC	This study	N/A
RT-PCR and qRT-PCR *rpl32* Reverse: ACGCACTCTGTTGTCGATACCCTT	This study	N/A
Software and algorithms		
Fiji/ImageJ	(Schindelin *et al.*, 2012; Rueden *et al.*, 2017)	https://imagej.net/
Integrated Genome Viewer (IGV)	(Robinson *et al.*, 2011)	https://igv.org/
Image Lab	Bio-Rad	https://image-lab-4-0.software.informer.com/
GraphPad (Prism)		

(*Continues*)

Reagent or resource	Source	Identifier
Other		
ChemiDoc	Bio-Rad	Catalogue no. 12003153
Humidified Incubators	Shel Lab	SRI20PF
#5 Dumont Fine Forceps	Ted Pella Inc.	Prod#5622
Motorized Pestle	Argos Technologies	Catalogue no. A0001
NanodropOne	Thermo Fisher Scientific	N/A

Resource availability

Lead contact. Further information and requests for resources and reagents should be directed to and will be fulfilled by the Lead Contact, Ken Moberg (kmoberg@emory.edu).

Materials availability

The *D. melanogaster* lines generated in this study are available by contacting the Lead Contact.

Data and code availability

This study did not generate any dataset or codes.

Experimental model and subject details

Flies (*D. melanogaster)* were raised on standard cornmeal agar medium and maintained in an incubator set at 25°C with a 12-h light/dark cycle. Crosses were reared under the same conditions, and standard medium was supplemented with dry yeast. The GAL4-UAS binary transgenic system was used to express transgenes of interest. Details of genotypes can be found in the Key Resources Table. One- to 5-day-old flies were used for experiments in this study. An equal number of males and females was used for all experiments.

Method details

D. melanogaster stocks and genetics. *D. melanogaster* stocks were raised on standard cornmeal agar and maintained in humidified incubators (SRI20PF, Shel Lab) at 25°C with 12-h light/dark cycles. Crosses were reared under the same conditions and supplemented with dry yeast. The strains used in this study are described in the Key Resources Table.

Viability and lifespan analysis. Viability at 25°C was measured by assessing eclosion rates of 100 wandering L3 larvae collected for each genotype, and then reared in a single vial. Hatching was recorded for 5–6 d. At least three independent biological replicates per genotype were tested for significance and calculated using group analysis on GraphPad (Prism). Lifespan was assessed at 25°C as described previously (Morton *et al*., 2020). In brief, newly eclosed flies were collected, placed in vials (10 flies per vial), and then transferred to fresh vials weekly, or as needed. Survivorship was scored daily. At least three independent biological replicates were tested for each genotype, and significance was calculated using group analysis on GraphPad (Prism).

Locomotion assays. Negative geotaxis was tested as previously described (Morton *et al*., 2020). Briefly, newly eclosed flies (day 0) were collected, and kept in vials for 2–5 d. Cohorts of 10 age-matched flies were transferred to a 25 ml graduated cylinder for analysis. Flies in graduated cylinders were tapped to bring flies to the bottom of the vial and the rate at which the flies traveled to the top of the vial (25 ml mark) was measured at 5, 10, 15, and 30 s). At least three biological replicates per genotype were analyzed and significance was calculated using grouped analysis on GraphPad (Prism).

Drosophila decapitation. CO_2-anesthetized flies were collected and frozen at −80°C for approximately five minutes. Frozen flies were then placed on a metal plate over dry ice. Gently, #5 Dumont fine forceps (Ted Pella, Inc.) were placed between the *Drosophila* head and thorax to remove the head from the remainder of the body. Heads were carefully placed in Eppendorf tubes, on ice, for subsequent processing.

RNA isolation for RT-PCR and real-time qPCR. Total RNA was isolated from ~25 adult fly heads using the TRIzol (Invitrogen) method. Briefly, *Drosophila* heads were homogenized in 0.1 ml TRIzol using a motorized pestle (Argos Technologies) on ice. TRIzol was added to samples to bring to a total volume of 0.5 ml and 0.1 ml of 1-Bromo-3-chloropropane (Scientific Laboratory Supplies) was added. Samples were vortexed on high speed for 10 s and incubated at room temperature for 15 min. Next, samples were centrifuged for 15 min at 13,000 × g at 4°C. The top, aqueous layer was removed and placed into a clean Eppendorf tube. An equal volume of 2-propanol (~250 μL) was added. Samples were inverted 10 times and incubated at room temperature for 10 min. Next, samples were centrifuged for 15 min at 13,000 × g at 4°C. The supernatant was removed, and 0.5 ml of 75% ethanol was added. Samples were centrifuged a final time for 15 min at 13,000 × g at 4°C. The supernatant was removed, and the samples were allowed to air dry until the remaining ethanol evaporated (~5 min). The pellet was resuspended in 10–20 μL of DEPC water. RNA concentration and purity was assessed using a Spectrophotometer (Thermo Fisher Scientific). Total RNA (1 μg) was treated with DNaseI (Qiagen). cDNA was generated using M-MLV Reverse Transcriptase (Invitrogen). Qiagen *Taq* polymerase (Qiagen) was used for PCR amplification of target transcripts and products were resolved and imaged on 1–2% agarose gels (Chemi-Doc). qRT-PCR reactions were carried out in technical triplicate with QuantiTect SYBR Green Master Mix using Applied Biosystems StepOne Plus real-time machine (ABI). Results were analyzed using ΔΔCT method, normalized to loading Control (e.g., *rpl32*), and plotted as relative levels normalized to Control. At least three independent biological replicates were performed for each genotype, and significance was calculated using group analysis on GraphPad (Prism). Primers used for all PCR reactions are listed in the Key Resources Table.

Immunoblotting. For analysis of Trio protein levels, ~25 adult fly heads (1–5 d old) were decapitated and collected on dry ice. Protein lysates were prepared by homogenizing heads in 0.5 ml of RIPA-2 Buffer (50 mM Tris-HCl, pH 8; 150 mM NaCl; 0.5% sodium deoxycholate; 1% Igepal CA-630 0.1% SDS) supplemented with protease inhibitors (1 mM PMSF; Pierce Protease Inhibitors; Thermo Fisher Scientific) and 1% SDS. Samples were sonicated 3 × 10 s with 1 min

on ice between repetitions, and then centrifuged at 13,000 × g for 15 min at 4°C. Protein lysate concentration was determined by Pierce BCA Protein Assay Kit (Life Technologies). Head lysate protein samples (40–60 µg) in reducing sample buffer (50 mM Tris-HCl, pH 6.8; 100 mM DTT; 2% SDS; 0.1% Bromophenol Blue; 10% glycerol) were resolved on 4–20% Criterion TGX Stain-Free Precast Polyacrylamide Gels (Bio-Rad), transferred to nitrocellulose membranes (Bio-Rad), and incubated for 1 h in blocking buffer (5% nonfat dry milk in 0.1% TBS-Tween) followed by overnight incubation with anti-Trio mAb (1:1000; DHSB #9.4A) diluted in blocking buffer. Primary antibody was detected using species-specific horseradish peroxidase conjugated secondary antibody (Jackson ImmunoResearch) with enhanced chemiluminescence (ECL, Sigma). Densitometry analysis was performed using Image Lab software (Bio-Rad). At least three independent biological replicates were performed for each genotype, and significance was calculated using group analysis on GraphPad (Prism).

***Drosophila* brain dissection, immunohistochemistry, visualization, and statistical analysis.** For *Drosophila* mushroom body morphology imaging, brains were dissected using #5 Dumont fine forceps (Ted Pella, Inc.) in PBS supplemented with 0.1% Triton X-100 (0.1% PBS-T). The proboscis was removed to provide a forceps grip point, and the remaining cuticle and trachea were peeled away from the brain. Brains were submerged in 1X PBS on ice until all brains were dissected. Dissected brains were fixed in 4% paraformaldehyde for 30 min and then permeabilized in 0.3% PBS-Triton X-100 (0.3% PBS-T) for 30 min, on ice. Brains were carefully transferred to 0.5 ml Eppendorf tubes in 0.1% PBS-T. For both primary and secondary antibody incubations, brains were left rocking at 4°C for 24–72 h (see list of dilutions and incubation times below) in 0.1% PBS-T supplemented with normal goat serum (Jackson ImmunoResearch) at a 1:20 dilution. Immunostained brains were mounted on SuperFrost Plus slides in Vectasheild (Vector Laboratories) using a coverslip bridge. Brains were imaged on a Nikon A1R confocal microscope. Approximately 25 brains were analyzed for each genotype, for each experiment. Maximum intensity projections were generated using Fiji ImageJ software.

Antibody: Mouse monoclonal 9.4A anti-Trio, **Incubation time:** 48–72 h, **Dilution:** 1:50

Antibody: Mouse monoclonal 1D4 anti-Fasciclin II, **Incubation time:** 48–72 h, **Dilution:** 1:50

Antibody: Rabbit Polyclonal Anti-Green Fluorescent Protein (GFP), **Incubation time:** Overnight-24 h, **Dilution:** 0.125:100

Antibody: Alexa Fluor 488 AffiniPure Polyclonal Goat Anti-rabbit IgG, **Incubation time:** Overnight-24 h, **Dilution:** 1:100

Antibody: Cy3 AffiniPure Polyclonal Goat Anti-Mouse IgG, **Incubation time:** Overnight-24 h, **Dilution:** 1:100

***Drosophila* neuron live imaging confocal microscopy, neuronal reconstruction, data analysis, and statistical analysis.** Live imaging of class IV ddaC neurons was performed as described previously (Iyer *et al.*, 2012). Briefly, ~10 wondering third instar *ppk-Gal4,UAS-mcd8::GFP*-labeled larvae were mounted in 1:5 (vol/vol) diethyl ether: halocarbon oil under an imaging bridge of 22 × 22 mm glass coverslips topped with a 22 × 55 mm glass coverslip. The ddaC images were captured on a Nikon A1R inverted Confocal microscope. Maximum intensity projections were generated using Fiji ImageJ software. Quantitative morphological data were compiled using the Simple Neurite tracer (SNT) plugin for Fiji (Ferreira *et al.*, 2014; Arshadi *et al.*, 2021). Batch processing was completed using a custom Fiji macro and Rstudio script created and gifted by Dr. Atit A. Patel (Dr. Dan Cox Lab, Georgia State University) (Lottes *et al.*, 2024) and the resulting data were exported to Excel (Microsoft).

Statistical analysis. Group analysis on biological triplicate experiments was performed using one-way or two-way ANOVA (Tukey's multiple-comparison test) on GraphPad (Prism). Sample sizes (n) and p-values are denoted in text, figures, and/or figure legends and indicated by asterisks (e.g., *, $p < 0.05$).

ACKNOWLEDGMENTS

This work was supported by the Emory University Emory Integrated Cellular Imaging Core Facility (RRID:SCR_023534). The authors thank Dr. Dan Cox, GA State Neuroscience Institute, and his lab members Drs. Erin Lottes and Atit Patel for training, reagents, and discussions. We also thank the members of the Moberg and Corbett laboratories, especially Dr. Milo Fasken for insightful discussions.

REFERENCES

Agrawal S, Kuo PH, Chu LY, Golzarroshan B, Jain M, Yuan HS (2019). RNA recognition motifs of disease-linked RNA-binding proteins contribute to amyloid formation. Sci Rep 9, 6171.

Alpert T, Straube K, Oesterreich FC, Herzel L, Neugebauer KM (2020). Widespread transcriptional readthrough caused by Nab2 depletion leads to chimeric transcripts with retained introns. Cell Rep 33, 108496.

Anderson JT, Wilson SM, Datar KV, Swanson MS (1993). NAB2: a yeast nuclear polyadenylated RNA-binding protein essential for cell viability. Mol Cell Biol 13, 2730–2741.

Arshadi C, Gunther U, Eddison M, Harrington KIS, Ferreira TA (2021). SNT: a unifying toolbox for quantification of neuronal anatomy. Nat Methods 18, 374–377.

Awasaki T, Saito M, Sone M, Suzuki E, Sakai R, Ito K, Hama C (2000). The Drosophila trio plays an essential role in patterning of axons by regulating their directional extension. Neuron 26, 119–131.

Ba W, Yan Y, Reijnders MR, Schuurs-Hoeijmakers JH, Feenstra I, Bongers EM, Bosch DG, De Leeuw N, Pfundt R, Gilissen C, *et al.* (2016). TRIO loss of function is associated with mild intellectual disability and affects dendritic branching and synapse function. Hum Mol Genet 25, 892–902.

Backer S, Lokmane L, Landragin C, Deck M, Garel S, Bloch-Gallego E (2018). Trio GEF mediates RhoA activation downstream of Slit2 and coordinates telencephalic wiring. Development 145, dev153692.

Banerjee A, Apponi LH, Pavlath GK, Corbett AH (2013). PABPN1: molecular function and muscle disease. FEBS J 280, 4230–4250.

Barbe B, Franke P, Maier W, Leboyer M (1996). Fragile X syndrome. I. An overview on its genetic mechanism. Eur Psychiatry 11, 227–232.

Bardoni B, Abekhoukh S, Zongaro S, Melko M (2012). Intellectual disabilities, neuronal posttranscriptional RNA metabolism, and RNA-binding proteins: three actors for a complex scenario. Prog Brain Res 197, 29–51.

Bateman J, Shu H, Van Vactor D (2000). The guanine nucleotide exchange factor trio mediates axonal development in the Drosophila embryo. Neuron 26, 93–106.

Bateman J, Van Vactor D (2001). The Trio family of guanine-nucleotide-exchange factors: regulators of axon guidance. J Cell Sci 114, 1973–1980.

Batisse J, Batisse C, Budd A, Bottcher B, Hurt E (2009). Purification of nuclear poly(A)-binding protein Nab2 reveals association with the yeast transcriptome and a messenger ribonucleoprotein core structure. J Biol Chem 284, 34911–34917.

Bellanger JM, Lazaro JB, Diriong S, Fernandez A, Lamb N, Debant A (1998a). The two guanine nucleotide exchange factor domains of Trio link the Rac1 and the RhoA pathways in vivo. Oncogene 16, 147–152.

Bellanger JM, Zugasti O, Lazaro JB, Diriong S, Lamb N, Sardet C, Debant A (1998b). [Role of the multifunctional Trio protein in the control of the Rac1 and RhoA gtpase signaling pathways]. C R Seances Soc Biol Fil 192, 367–374.

Bienkowski RS, Banerjee A, Rounds JC, Rha J, Omotade OF, Gross C, Morris KJ, Leung SW, Pak C, Jones SK, *et al.* (2017). The conserved, disease-associated RNA binding protein dNab2 interacts with the fragile X protein ortholog in Drosophila neurons. Cell Rep 20, 1372–1384.

Bircher JE, Koleske AJ (2021). Trio family proteins as regulators of cell migration and morphogenesis in development and disease - mechanisms and cellular contexts. J Cell Sci 134, jcs248393.
Brais B (2003). Oculopharyngeal muscular dystrophy: a late-onset polyalanine disease. Cytogenet Genome Res 100, 252–260.
Briancon-Marjollet A, Ghogha A, Nawabi H, Triki I, Auziol C, Fromont S, Piche C, Enslen H, Chebli K, Cloutier JF, *et al.* (2008). Trio mediates netrin-1-induced Rac1 activation in axon outgrowth and guidance. Mol Cell Biol 28, 2314–2323.
Conlon EG, Manley JL (2017). RNA-binding proteins in neurodegeneration: mechanisms in aggregate. Genes Dev 31, 1509–1528.
Cooper TA, Wan L, Dreyfuss G (2009). RNA and disease. Cell 136, 777–793.
Corbett AH (2018). Post-transcriptional regulation of gene expression and human disease. Curr Opin Cell Biol 52, 96–104.
Corgiat EB, List SM, Rounds JC, Corbett AH, Moberg KH (2021). The RNA-binding protein Nab2 regulates the proteome of the developing Drosophila brain. J Biol Chem 297, 100877.
Corgiat EB, List SM, Rounds JC, Yu D, Chen P, Corbett AH, Moberg KH (2022). The Nab2 RNA-binding protein patterns dendritic and axonal projections through a planar cell polarity-sensitive mechanism. G3 (Bethesda) 12, jkac100.
Corley M, Burns MC, Yeo GW (2020). How RNA-binding proteins interact with RNA: Molecules and mechanisms. Mol Cell 78, 9–29.
Crittenden JR, Skoulakis EM, Han KA, Kalderon D, Davis RL (1998). Tripartite mushroom body architecture revealed by antigenic markers. Learn Mem 5, 38–51.
Currey HN, Kraemer BC, Liachko NF (2023). *sut-2* loss of function mutants protect against tau-driven shortened lifespan and hyperactive pharyngeal pumping in a *C. elegans* model of tau toxicity. MicroPubl Biol 2023.
Darnell JC, Richter JD (2012). Cytoplasmic RNA-binding proteins and the control of complex brain function. Cold Spring Harb Perspect Biol 4, a012344.
Debant A, Serra-Pages C, Seipel K, O'Brien S, Tang M, Park SH, Streuli M (1996). The multidomain protein Trio binds the LAR transmembrane tyrosine phosphatase, contains a protein kinase domain, and has separate rac-specific and rho-specific guanine nucleotide exchange factor domains. Proc Natl Acad Sci USA 93, 5466–5471.
DeGeer J, Kaplan A, Mattar P, Morabito M, Stochaj U, Kennedy TE, Debant A, Cayouette M, Fournier AE, Lamarche-Vane N (2015). Hsc70 chaperone activity underlies Trio GEF function in axon growth and guidance induced by netrin-1. J Cell Biol 210, 817–832.
Edens BM, Ajroud-Driss S, Ma L, Ma YC (2015). Molecular mechanisms and animal models of spinal muscular atrophy. Biochim Biophys Acta 1852, 685–692.
Fasken MB, Corbett AH, Stewart M (2019). Structure-function relationships in the Nab2 polyadenosine-RNA binding Zn finger protein family. Protein Sci 28, 513–523.
Ferreira TA, Blackman AV, Oyrer J, Jayabal S, Chung AJ, Watt AJ, Sjostrom PJ, van Meyel DJ (2014). Neuronal morphometry directly from bitmap images. Nat Methods 11, 982–984.
Franke P, Barbe B, Leboyer M, Maier W (1996). Fragile X syndrome. II. Cognitive and behavioral correlates of mutations of the FMR-1 gene. Eur Psychiatry 11, 233–243.
Fushima K, Tsujimura H (2007). Precise control of fasciclin II expression is required for adult mushroom body development in Drosophila. Dev Growth Differ 49, 215–227.
Gebauer F, Schwarzl T, Valcarcel J, Hentze MW (2021). RNA-binding proteins in human genetic disease. Nat Rev Genet 22, 185–198.
Goss DJ, Kleiman FE (2013). Poly(A) binding proteins: Are they all created equal? Wiley Interdiscip Rev RNA 4, 167–179.
Green DM, Marfatia KA, Crafton EB, Zhang X, Cheng X, Corbett AH (2002). Nab2p is required for poly(A) RNA export in Saccharomyces cerevisiae and is regulated by arginine methylation via Hmt1p. J Biol Chem 277, 7752–7760.
Grenier St-Sauveur V, Soucek S, Corbett AH, Bachand F (2013). Poly(A) tail-mediated gene regulation by opposing roles of Nab2 and Pab2 nuclear poly(A)-binding proteins in pre-mRNA decay. Mol Cell Biol 33, 4718–4731.
Gross C, Berry-Kravis EM, Bassell GJ (2012). Therapeutic strategies in fragile X syndrome: Dysregulated mGluR signaling and beyond. Neuropsychopharmacology 37, 178–195.
Guthrie CR, Greenup L, Leverenz JB, Kraemer BC (2011). MSUT2 is a determinant of susceptibility to tau neurotoxicity. Hum Mol Genet 20, 1989–1999.
Guthrie CR, Schellenberg GD, Kraemer BC (2009). SUT-2 potentiates tau-induced neurotoxicity in Caenorhabditis elegans. Hum Mol Genet 18, 1825–1838.
Haussmann IU, Bodi Z, Sanchez-Moran E, Mongan NP, Archer N, Fray RG, Soller M (2016). m(6)A potentiates Sxl alternative pre-mRNA splicing for robust Drosophila sex determination. Nature 540, 301–304.
Hector RE, Nykamp KR, Dheur S, Anderson JT, Non PJ, Urbinati CR, Wilson SM, Minvielle-Sebastia L, Swanson MS (2002). Dual requirement for yeast hnRNP Nab2p in mRNA poly(A) tail length control and nuclear export. EMBO J 21, 1800–1810.
Heisenberg M (1998). What do the mushroom bodies do for the insect brain? An introduction. Learn Mem 5, 1–10.
Heisenberg M (2003). Mushroom body memoir: from maps to models. Nat Rev Neurosci 4, 266–275.
Iyer SC, Wang D, Iyer EP, Trunnell SA, Meduri R, Shinwari R, Sulkowski MJ, Cox DN (2012). The RhoGEF trio functions in sculpting class specific dendrite morphogenesis in Drosophila sensory neurons. PLoS One 7, e33634.
Jaffe AB, Hall A (2005). Rho GTPases: Biochemistry and biology. Annu Rev Cell Dev Biol 21, 247–269.
Jalloh B, Lancaster CL, Rounds JC, Brown BE, Leung SW, Banerjee A, Morton DJ, Bienkowski RS, Fasken MB, Kremsky IJ, *et al.* (2023). The Drosophila Nab2 RNA binding protein inhibits m(6)A methylation and male-specific splicing of Sex lethal transcript in female neuronal tissue. Elife 12, e64904.
Jones SK, Rha J, Kim S, Morris KJ, Omotade OF, Moberg KH, Myers KR, Corbett AH (2020). The polyadenosine RNA binding protein ZC3H14 is required in mice for proper dendritic spine density. bioRxiv.
Kahsai L, Zars T (2011). Learning and memory in Drosophila: Behavior, genetics, and neural systems. Int Rev Neurobiol 99, 139–167.
Kan L, Grozhik AV, Vedanayagam J, Patil DP, Pang N, Lim KS, Huang YC, Joseph B, Lin CJ, Despic V, *et al.* (2017). The m(6)A pathway facilitates sex determination in Drosophila. Nat Commun 8, 15737.
Kan L, Ott S, Joseph B, Park ES, Dai W, Kleiner RE, Claridge-Chang A, Lai EC (2021). A neural m(6)A/Ythdf pathway is required for learning and memory in Drosophila. Nat Commun 12, 1458.
Katrancha SM, Shaw JE, Zhao AY, Myers SA, Cocco AR, Jeng AT, Zhu M, Pittenger C, Greer CA, Carr SA, *et al.* (2019). Trio haploinsufficiency causes neurodevelopmental disease-associated deficits. Cell Rep 26, 2805–2817.e2809.
Katrancha SM, Wu Y, Zhu M, Eipper BA, Koleske AJ, Mains RE (2017). Neurodevelopmental disease-associated de novo mutations and rare sequence variants affect TRIO GDP/GTP exchange factor activity. Hum Mol Genet 26, 4728–4740.
Kelly S, Pak C, Garshasbi M, Kuss A, Corbett AH, Moberg K (2012). New kid on the ID block: Neural functions of the Nab2/ZC3H14 class of Cys(3) His tandem zinc-finger polyadenosine RNA binding proteins. RNA Biol 9, 555–562.
Kelly SM, Bienkowski R, Banerjee A, Melicharek DJ, Brewer ZA, Marenda DR, Corbett AH, Moberg KH (2016). The Drosophila ortholog of the Zc3h14 RNA binding protein acts within neurons to pattern axon projection in the developing brain. Dev Neurobiol 76, 93–106.
Kelly SM, Leung SW, Apponi LH, Bramley AM, Tran EJ, Chekanova JA, Wente SR, Corbett AH (2010). Recognition of polyadenosine RNA by the zinc finger domain of nuclear poly(A) RNA-binding protein 2 (Nab2) is required for correct mRNA 3'-end formation. J Biol Chem 285, 26022–26032.
Kelly SM, Leung SW, Pak C, Banerjee A, Moberg KH, Corbett AH (2014). A conserved role for the zinc finger polyadenosine RNA binding protein, ZC3H14, in control of poly(A) tail length. RNA 20, 681–688.
Kelly SM, Pabit SA, Kitchen CM, Guo P, Marfatia KA, Murphy TJ, Corbett AH, Berland KM (2007). Recognition of polyadenosine RNA by zinc finger proteins. Proc Natl Acad Sci USA 104, 12306–12311.
Kolb SJ, Kissel JT (2011). Spinal muscular atrophy: A timely review. Arch Neurol 68, 979–984.
Lage K, Hansen NT, Karlberg EO, Eklund AC, Roque FS, Donahoe PK, Szallasi Z, Jensen TS, Brunak S (2008). A large-scale analysis of tissue-specific pathology and gene expression of human disease genes and complexes. Proc Natl Acad Sci USA 105, 20870–20875.
Lee WH, Corgiat E, Rounds JC, Shepherd Z, Corbett AH, Moberg KH (2020). A genetic screen links the disease-associated Nab2 RNA-binding protein to the planar cell polarity pathway in Drosophila melanogaster. G3 (Bethesda) 10, 3575–3583.
Leeuwen FN, Kain HE, Kammen RA, Michiels F, Kranenburg OW, Collard JG (1997). The guanine nucleotide exchange factor Tiam1 affects neuronal

morphology; opposing roles for the small GTPases Rac and Rho. J Cell Biol 139, 797–807.
Lence T, Akhtar J, Bayer M, Schmid K, Spindler L, Ho CH, Kreim N, Andrade-Navarro MA, Poeck B, Helm M, Roignant JY (2016). m(6)A modulates neuronal functions and sex determination in Drosophila. Nature 540, 242–247.
Leung SW, Apponi LH, Cornejo OE, Kitchen CM, Valentini SR, Pavlath GK, Dunham CM, Corbett AH (2009). Splice variants of the human ZC3H14 gene generate multiple isoforms of a zinc finger polyadenosine RNA binding protein. Gene 439, 71–78.
Lottes EN, Ciger F, Bhattacharjee S, Timmins EA, Tete B, Tran T, Matta J, Patel AA, Cox DN (2024). CCT and Cullin1 regulate the TORC1 pathway to promote dendritic arborization in health and disease. Cells 13, 1029.
Luo S, Tong L (2014). Molecular basis for the recognition of methylated adenines in RNA by the eukaryotic YTH domain. Proc Natl Acad Sci USA 111, 13834–13839.
Maniatis T, Reed R (2002). An extensive network of coupling among gene expression machines. Nature 416, 499–506.
Marfatia KA, Crafton EB, Green DM, Corbett AH (2003). Domain analysis of the Saccharomyces cerevisiae heterogeneous nuclear ribonucleoprotein, Nab2p. Dissecting the requirements for Nab2p-facilitated poly(A) RNA export. J Biol Chem 278, 6731–6740.
McKee AE, Silver PA (2007). Systems perspectives on mRNA processing. Cell Res 17, 581–590.
McMillan PJ, Strovas TJ, Baum M, Mitchell BK, Eck RJ, Hendricks N, Wheeler JM, Latimer CS, Keene CD, Kraemer BC (2021). Pathological tau drives ectopic nuclear speckle scaffold protein SRRM2 accumulation in neuron cytoplasm in Alzheimer's disease. Acta Neuropathol Commun 9, 117.
Morton DJ, Jalloh B, Kim L, Kremsky I, Nair RJ, Nguyen KB, Rounds JC, Sterrett MC, Brown B, Le T, *et al.* (2020). A Drosophila model of Pontocerebellar Hypoplasia reveals a critical role for the RNA exosome in neurons. PLoS Genet 16, e1008901.
Newsome TP, Schmidt S, Dietzl G, Keleman K, Asling B, Debant A, Dickson BJ (2000). Trio combines with dock to regulate Pak activity during photoreceptor axon pathfinding in Drosophila. Cell 101, 283–294.
Pak C, Garshasbi M, Kahrizi K, Gross C, Apponi LH, Noto JJ, Kelly SM, Leung SW, Tzschach A, Behjati F, *et al.* (2011). Mutation of the conserved polyadenosine RNA binding protein, ZC3H14/dNab2, impairs neural function in Drosophila and humans. Proc Natl Acad Sci USA 108, 12390–12395.
Paskus JD, Herring BE, Roche KW (2020). Kalirin and Trio: RhoGEFs in synaptic transmission, plasticity, and complex brain disorders. Trends Neurosci 43, 505–518.
Patil DP, Pickering BF, Jaffrey SR (2018). Reading m(6)A in the transcriptome: m(6)A-binding proteins. Trends Cell Biol 28, 113–127.
Peng YJ, He WQ, Tang J, Tao T, Chen C, Gao YQ, Zhang WC, He XY, Dai YY, Zhu NC, *et al.* (2010). Trio is a key guanine nucleotide exchange factor coordinating regulation of the migration and morphogenesis of granule cells in the developing cerebellum. J Biol Chem 285, 24834–24844.
Pengelly RJ, Greville-Heygate S, Schmidt S, Seaby EG, Jabalameli MR, Mehta SG, Parker MJ, Goudie D, Fagotto-Kaufmann C, Mercer C, *et al.* (2016). Mutations specific to the Rac-GEF domain of TRIO cause intellectual disability and microcephaly. J Med Genet 53, 735–742.
Pirozzi F, Tabolacci E, Neri G (2011). The FRAXopathies: Definition, overview, and update. Am J Med Genet A 155A, 1803–1816.
Portales-Casamar E, Briancon-Marjollet A, Fromont S, Triboulet R, Debant A (2006). Identification of novel neuronal isoforms of the Rho-GEF Trio. Biol Cell 98, 183–193.
Rha J, Jones SK, Fidler J, Banerjee A, Leung SW, Morris KJ, Wong JC, Inglis GAS, Shapiro L, Deng Q, *et al.* (2017). The RNA-binding protein, ZC3H14, is required for proper poly(A) tail length control, expression of synaptic proteins, and brain function in mice. Hum Mol Genet 26, 3663–3681.
Robinson JT, Thorvaldsdottir H, Wenger AM, Zehir A, Mesirov JP (2017). Variant review with the Integrative Genomics Viewer. Cancer Res 77, e31–e34.
Robinson JT, Thorvaldsdottir H, Winckler W, Guttman M, Lander ES, Getz G, Mesirov JP (2011). Integrative Genomics Viewer. Nat Biotechnol 29, 24–26.
Roman G, Davis RL (2001). Molecular biology and anatomy of Drosophila olfactory associative learning. Bioessays 23, 571–581.
Rounds JC, Corgiat EB, Ye C, Behnke JA, Kelly SM, Corbett AH, Moberg KH (2021). The disease-associated proteins *Drosophila* Nab2 and Ataxin-2 interact with shared RNAs and coregulate neuronal norphology. bioRxiv.
Rounds JC, Corgiat EB, Ye C, Behnke JA, Kelly SM, Corbett AH, Moberg KH (2022). The disease-associated proteins Drosophila Nab2 and Ataxin-2 interact with shared RNAs and coregulate neuronal morphology. Genetics 220, iyab175.
Rueden CT, Schindelin J, Hiner MC, DeZonia BE, Walter AE, Arena ET, Eliceiri KW (2017). ImageJ2: ImageJ for the next generation of scientific image data. BMC Bioinformatics 18, 529.
Santoro MR, Bray SM, Warren ST (2012). Molecular mechanisms of fragile X syndrome: a twenty-year perspective. Annu Rev Pathol 7, 219–245.
Schindelin J, Arganda-Carreras I, Frise E, Kaynig V, Longair M, Pietzsch T, Preibisch S, Rueden C, Saalfeld S, Schmid B, *et al.* (2012). Fiji: An open-source platform for biological-image analysis. Nat Methods 9, 676–682.
Schmid M, Olszewski P, Pelechano V, Gupta I, Steinmetz LM, Jensen TH (2015). The nuclear PolyA-binding protein Nab2p is essential for mRNA production. Cell Rep 12, 128–139.
Shivalkar M, Giniger E (2012). Control of dendritic morphogenesis by Trio in Drosophila melanogaster. PLoS One 7, e33737.
Song JK, Giniger E (2011). Noncanonical Notch function in motor axon guidance is mediated by Rac GTPase and the GEF1 domain of Trio. Dev Dyn 240, 324–332.
Soucek S, Zeng Y, Bellur DL, Bergkessel M, Morris KJ, Deng Q, Duong D, Seyfried NT, Guthrie C, Staley JP, *et al.* (2016). The evolutionarily-conserved polyadenosine RNA binding protein, Nab2, cooperates with splicing machinery to regulate the fate of pre-mRNA. Mol Cell Biol 36, 2697–2714.
Takemura SY, Aso Y, Hige T, Wong A, Lu Z, Xu CS, Rivlin PK, Hess H, Zhao T, Parag T, *et al.* (2017). A connectome of a learning and memory center in the adult Drosophila brain. Elife 6, e26975.
Thelen MP, Kye MJ (2019). The role of RNA binding proteins for local mRNA translation: Implications in neurological disorders. Front Mol Biosci 6, 161.
Theler D, Dominguez C, Blatter M, Boudet J, Allain FH (2014). Solution structure of the YTH domain in complex with N6-methyladenosine RNA: A reader of methylated RNA. Nucleic Acids Res 42, 13911–13919.
Wan L, Dockendorff TC, Jongens TA, Dreyfuss G (2000). Characterization of dFMR1, a Drosophila melanogaster homolog of the fragile X mental retardation protein. Mol Cell Biol 20, 8536–8547.
Wheeler JM, McMillan P, Strovas TJ, Liachko NF, Amlie-Wolf A, Kow RL, Klein RL, Szot P, Robinson L, Guthrie C, *et al.* (2019). Activity of the poly(A) binding protein MSUT2 determines susceptibility to pathological tau in the mammalian brain. Sci Transl Med 11, eaao6545.
Wigington CP, Williams KR, Meers MP, Bassell GJ, Corbett AH (2014). Poly(A) RNA-binding proteins and polyadenosine RNA: New members and novel functions. Wiley Interdiscip Rev RNA 5, 601–622.
Worpenberg L, Paolantoni C, Longhi S, Mulorz MM, Lence T, Wessels HH, Dassi E, Aiello G, Sutandy FXR, Scheibe M, *et al.* (2021). Ythdf is a N6-methyladenosine reader that modulates Fmr1 target mRNA selection and restricts axonal growth in Drosophila. EMBO J 40, e104975.
Xu C, Liu K, Ahmed H, Loppnau P, Schapira M, Min J (2015). Structural basis for the discriminative recognition of N6-methyladenosine RNA by the human YT521-B homology domain family of proteins. J Biol Chem 290, 24902–24913.
Xu C, Wang X, Liu K, Roundtree IA, Tempel W, Li Y, Lu Z, He C, Min J (2014). Structural basis for selective binding of m6A RNA by the YTHDC1 YTH domain. Nat Chem Biol 10, 927–929.
Yagi R, Mabuchi Y, Mizunami M, Tanaka NK (2016). Convergence of multimodal sensory pathways to the mushroom body calyx in Drosophila melanogaster. Sci Rep 6, 29481.